AD A091509

UNCLASSIFIED

SECURITY CLASSIFICATION OF THIS PAGE (When Data Entered)

REPORT DOCUMENTATION PAGE

READ INSTRUCTIONS BEFORE COMPLETING FORM

1. REPORT NUMBER: HDL-TR-1931	2. GOVT ACCESSION NO.: AD-A092 509
3. RECIPIENT'S CATALOG NUMBER	
4. TITLE (and Subtitle): A Near-Surface Burst EMP Driver Package for Prompt Gamma-Induced Sources	5. TYPE OF REPORT & PERIOD COVERED: Technical Report
6. PERFORMING ORG. REPORT NUMBER	
7. AUTHOR(s): William T. Wyatt, Jr.	8. CONTRACT OR GRANT NUMBER(s): DA: 1L162120AH25
9. PERFORMING ORGANIZATION NAME AND ADDRESS: Harry Diamond Laboratories, 2800 Powder Mill Road, Adelphi, MD 20783	10. PROGRAM ELEMENT, PROJECT, TASK AREA & WORK UNIT NUMBERS: Prog. El.: 6.21.20.A
11. CONTROLLING OFFICE NAME AND ADDRESS: U.S. Army Materiel Development and Readiness Command, Alexandria, VA 22333	12. REPORT DATE: Sep[illegible]1980
	13. NUMBER OF PAGES: 50
14. MONITORING AGENCY NAME & ADDRESS (if different from Controlling Office)	15. SECURITY CLASS. (of this report): UNCLASSIFIED
	15a. DECLASSIFICATION/DOWNGRADING SCHEDULE

16. DISTRIBUTION STATEMENT (of this Report)

Approved for public release; distribution unlimited.

17. DISTRIBUTION STATEMENT (of the abstract entered in Block 20, if different from Report)

18. SUPPLEMENTARY NOTES

HDL Project: X750E6
DRCMS Code: 612120.H250011

19. KEY WORDS (Continue on reverse side if necessary and identify by block number)

EMP	Electromagnetic pulse	Curve fitting
Compton currents	Radiation transport	
Nuclear explosions	Monte Carlo method	
Gamma rays	Computer codes	

20. ABSTRACT (Continue on reverse side if necessary and identify by block number)

This report summarizes the development of a software package specifying electromagnetic pulse (EMP) drivers produced by prompt gamma rays emitted by a near-surface nuclear burst in the air. The package is designed for use with the NEMP EMP prediction computer code. This report describes improved calculations of EMP drivers arising from a point gamma source in air over ground, based on Monte Carlo simulation of the gamma transport by the specially

DD FORM 1 JAN 73 1473 EDITION OF 1 NOV 65 IS OBSOLETE 1 UNCLASSIFIED

SECURITY CLASSIFICATION OF THIS PAGE (When Data Entered)

163050 slh

20. Abstract (Cont'd)

developed SLEDGE computer code. This simulation was done for seven source gamma energies from 0.5 to 7.0 MeV. The transport was carried to a range of 25 mean free paths. Correlated sampling was used to estimate Compton electron currents more accurately. The theoretical basis of the SLEDGE code is discussed. Analytic approximations to the Monte Carlo results are described in detail, including (1) the energy deposition buildup factor (both free field and ground influenced), (2) time dependence of energy deposition as a function of both range from the burst and nearness to the ground, (3) ratio of radial Compton electron current to energy deposition rate, and (4) theta Compton electron current due to the presence of the ground. Comparisons are made with two previous EMP driver packages, with good agreement for cases where the previous packages are believed reliable.

FOREWORD

The nuclear electromagnetic pulse (EMP) is a transient broadband electromagnetic field capable of damaging or upsetting electronic equipment on the tactical nuclear battlefield. To predict the signature of the EMP generated by a nuclear burst, it is necessary to determine the EMP drivers--time and space varying ionization and Compton electron currents in the nuclear radiation field around the burst. Once the ionization and Compton currents are specified, it is usually possible to solve some form of Maxwell's equations for the EMP generated.

This report summarizes the development of a software package specifying EMP drivers produced by prompt gamma rays emitted by a near-surface burst in the air. The package was designed for use with the NEMP EMP environment prediction computer code used at the Harry Diamond Laboratories. A separate report, A Near-Surface Burst EMP Driver Package for Neutron-Induced Sources, HDL-TR-1930 (September 1980), summarizes the development of a similar software package for EMP drivers due to neutrons and neutron-induced secondary gamma rays.

Part I of this report describes the development of the Monte Carlo gamma ray transport computer code and data base to be fitted. Part II describes the curve-fitting exercise and compares these results with earlier results.

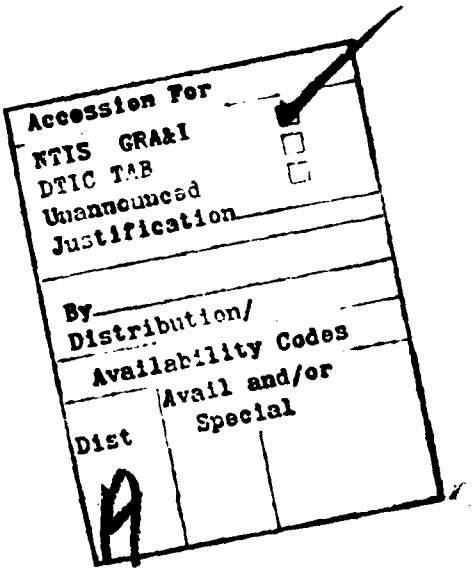

CONTENTS

CONTENTS (Cont'd)

FIGURES

FIGURES (Cont'd)

TABLES

PART I. EMP DRIVERS FROM GAMMA TRANSPORT BY MONTE CARLO

1. REQUIREMENTS FOR NEW EMP DRIVER AND GAMMA TRANSPORT DATA

Electromagnetic pulse (EMP) drivers consist of one component arising from prompt gamma radiation and a second component arising from neutron radiation. The NEMP computer code[1,2] obtains the solution of Maxwell's equations for EMP from a near-surface burst in the air. The EMP drivers must be incorporated into the NEMP code as smooth fits to quasi-analytic or Monte Carlo predictions. Earlier EMP driver fits were used in the LEMP computer code[3] for EMP from surface bursts. The LEMP prompt gamma ray EMP drivers were used in the NEMP code at first, but a quick-look Monte Carlo study by this author confirmed several deficiencies in these LEMP drivers:

a. Incorrect range dependence for the gamma ray buildup factor at more than about five gamma ray attenuation lengths penetration, becoming exponentially worse at deeper penetrations

b. Incorrect time dependence at deeper penetrations (LEMP drivers' time dependence is independent of range and decreases with time too rapidly at deeper penetrations.)

c. Lack of a ground effect on the buildup factor (The ground actually inhibits the increase of the buildup factor with range for observers near the ground.)

d. Lack of late vertical Compton currents induced by the effect of the ground on gamma transport

It was therefore decided to develop newer, more realistic drivers for the NEMP code that would overcome these deficiencies and also account for the effect of a nonzero burst height. The new drivers would be valid to a penetration depth of at least 20 gamma ray attenuation lengths and would encompass more discrete gamma ray energies than the LEMP drivers (which included 0.5-, 1.5-, and 5.0-MeV gamma ray sources). The new drivers would use the same LEMP philosophy of using well-chosen analytic functionals to describe time and space dependence of the data, in preference to using piecewise polynomial fits.

---

[1] *H. J. Longley, C. L. Longmire, and K. S. Smith, Development of NEMP (U), Mission Research Corp., Santa Barbara, CA, HDL-CR-75-001-1 (April 1975). (SECRET--RESTRICTED DATA)*

[2] *H. J. Longley and K. S. Smith, Developments in NEMP for 1977 (U), Mission Research Corp., Santa Barbara, CA, HDL-CR-77-0022-1 (January 1978). (SECRET--RESTRICTED DATA)*

[3] *H. J. Longley and C. L. Longmire, Development and Testing of LEMP 1, Los Alamos Scientific Laboratory, NM, LA-4346 (April 1970).*

2. DEVELOPMENT OF SLEDGE, A MONTE CARLO GAMMA TRANSPORT CODE

To first test the validity of the LEMP drivers and then obtain needed, more detailed predictions of EMP drivers, it was decided to write a special-purpose Monte Carlo code for gamma ray transport, specially tailored for efficiency in calculating the data needed. The code was written in FORTRAN IV and run on the Harry Diamond Laboratories (HDL) computer (an IBM System/370 Model 168). The code consists of several thousand FORTRAN statements and includes 53 program and subprogram units. It was named SLEDGE, after the basic tool for realigning existing structures; "SLEDGE" is also an acronym for "surface and low-altitude EMP drivers due to gamma emission." An overview of the SLEDGE code is presented here with additional detail on innovations or other important aspects.

The SLEDGE code models time-dependent gamma ray transport from a point source in air-over-ground cylindrical geometry. The collision kernel includes Compton scattering, photoabsorption, and pair production. Time dependence is maintained in retarded time from the source point (the nuclear burst). For this study, the gamma ray source was monochromatic in energy and a delta function in time.

The gamma ray flux is sampled to obtain the desired EMP driver response functions--electron current vector and energy deposition rate. Energy deposition and radial and theta components of the electron current vector are scored within volume detectors by both track-length and collision estimators of the gamma ray flux and are scored at the surfaces of volume detectors by a boundary crossing estimator of the gamma ray flux. Optionally, collision estimator scoring can be done in spherical polar coordinate radial bins to obtain one-dimensional (1-d) results. Thus, removal of the ground allows spherically symmetric free-field results to be accumulated in the 1-d radial bins. Inclusion of the ground allows azimuthally symmetric, ground-influenced results to be accumulated in the 2-d cylindrical geometry volume detectors.

The random walk permits exponential transform biasing, angular and energy biasing of the source, and directional biasing of gamma rays emerging from Compton collisions. Splitting can be done to prevent growth of particle weight due to biasing at collisions or at transports. Splitting and roulette can be used in connection with detector importances to improve statistics in desired regions (zone splitting). Splitting and roulette can be used also to reduce the variance of gamma ray weights in specifiable detectors (weight balancing). A special technique may be used to greatly reduce the variance of the ratio of electron current to energy deposition rate, based on the (early time) correlation between the electron currents and the energy deposition.

2.1 Random Walk and Estimator Scoring

After reading problem input, setting up time and space meshes, and initializing necessary tables, the SLEDGE code executes a batch loop and then scans the results of each batch to develop grand totals and batch statistics. Each batch consists of a particle (gamma ray) history loop followed by saving the total results for the batch. A typical production run of 30,000 histories might consist of 20 batches of 1500 histories each. Each particle history consists of identifying a particle and all its subparticles created by splitting and following them through successive random walks until extinction. The random walk consists of these steps:

(1) Generating the particle or subparticle

(2) Determining the number of mean free paths down which the particle is to be transported prior to a collision

(3) Tracking the particle through space and time to the collision point, while scoring track-length or surface crossing estimators for the detectors encountered

(4) Colliding the particle to obtain the emergent particle energy and direction, while scoring collision estimators for the detector involved, and then repeating steps (2), (3), and (4) until extinction

The particle or subparticle can be killed or split after step (2) or (3) or (4) through photoabsorption, escape, age cutoff, low energy cutoff, collision number limit, or any of the roulette or splitting mechanisms. Subparticles produced are stored in a split stack and are withdrawn one at a time from the split stack in step (1). Ultimately, there are no entries remaining in the split stack, and the next particle history can be started.

Many standard techniques were drawn from the literature, particularly from Carter and Cashwell.[4]

Generating the particle involves determining its position (at the burst), direction cosines (usually biased), energy (simply monochromatic in this study), age, and weight.

Determining the number of mean free paths, N, was done by

$$N = - \ell n \, (\xi)$$

[4] *L. L. Carter and E. D. Cashwell, Particle-Transport Simulation with the Monte Carlo Method, U.S. Energy Research and Development Administration TID-26607 (1975).*

for a uniform random number, ξ, selected from the interval (0,1). A rejection method was used to eliminate escapes before the first scatter for a particle. Both exponential transform and importance function biasing were used for first-scatter transport, and exponential transform biasing was used for later scatters. These are discussed in more detail in section 2.2.

Tracking the particle involved finding its track-length in the detector that it was inside (detector volumes being mutually exclusive and filling all space within the grid outer boundary), scoring track-length and surface crossing estimators, moving the particle to the next detector, and repeating the process until the particle reached a collision point or was killed. When the particle reached a collision point, the 2-d and 1-d collision estimators were scored, also.

Standard means were used to select the collision event from Compton collision, photoabsorption, and pair production probabilities. Pair production was assumed isotropic. Standard algorithms were used to select the emergent energy and the direction of Compton scattered gamma rays. Emergent direction biasing could be used, as described in section 2.2.

The track-length estimation of the flux, F (that is, path length per unit volume), is

$$F = pW_{BC}/V \ ,$$

where p is the track-length in the particular volume detector and time bin, W_{BC} is the particle weight before collision, and V is the detector volume. The electron current magnitude, J, is

$$J = F\left(R_c/\lambda_c + R_p/\lambda_p\right) \ ,$$

where R_c is the average forward range of Compton electrons (for the incident gamma ray energy), λ_c is the Compton collision or attenuation length, R_p is the average forward range of photoelectrons, and λ_p is the photoelectric absorption length. R_c was computed and tabulated by the SLEDGE code by using the Compton differential scattering cross section and the electron range-energy relation in air. R_p was adapted from the literature. The energy deposition, D, is

$$D = F\left[E/\lambda_a + E/\lambda_p + (E - 1.022)/\lambda_{pp}\right] \ ,$$

where E is the gamma ray energy in MeV, λ_a is the Compton absorption length, and λ_{pp} is the pair production absorption length.

Once J is obtained, it is decomposed into radial and vertical components.

The surface crossing estimation of the flux, scored only when the surface is crossed, is

$$F = W_{BC}/CA \ ,$$

where C is the sine of the angle between the surface and the particle direction and A is the area of the surface. J and D are derived as before.

The collision estimation of the flux, scored only when a collision point is reached, is

$$F = W_{BC}/\sigma V \ ,$$

where σ is the total collision cross section in the detector with volume V. J and D are derived as before.

The time bin associated with scoring surface crossing and collision estimators is simple to determine. However, for the track-length estimator, the particle may pass through several time bins while traversing a detector volume. The portion of the track-length spent in each time bin must be determined to score the time dependence properly. Although this determination requires somewhat more computer time, the associated variance is usually much better for the track-length estimator. Generally, all three estimators were used to check for agreement and insure correct results.

No account was taken of the effect of the ground upon the transport of Compton electrons and photoelectrons. Some effects would be expected within roughly 1 m of the ground. This effect could be a fruitful subject for future study.

2.2 Biasing and Importance Functions

The analog model of gamma ray transport (that is, no biasing or importance functions) is useless for deep penetration problems. Some means must be used to force gamma rays to penetrate to distant regions in large enough numbers to produce useful, low variance results. A number of methods were tested in the SLEDGE code for the problems under consideration. These may be categorized as (1) source biasing, (2) transport biasing, and (3) collision biasing, modifying respectively the source function, the transport kernel, or the collision kernel of the transport integral. Two risks are associated with the use of properly normalized biasing methods:

a. The variance of the flux may be infinite or possibly very large so that as the number of batches increases, the variance gets larger, not smaller.

b. The transport integral (integrated over position, velocity, time, and energy) may be undersampled since strong biasing may force the sampling away from portions of the integral space that contribute significantly to the correct answer.

Thus, the biasing methods must be properly constructed and not overused and yet must be powerful enough to be worth the trouble of using. In general, source biasing very effectively reduces the variance in deep penetration problems. Also, splitting with roulette is a simple but highly effective method for transport biasing. In this study, collision biasing was only of minor importance in variance reduction.

2.2.1 Source Biasing

Source directional biasing was not used in the SLEDGE code to obtain 1-d results. However, for the 2-d air-over-ground studies, source directional biasing was used by construction of a cumulative distribution function (cdf) based on a nonisotropic importance function. Conventional cylindrical coordinates (ρ,z,ϕ) are used, where z is positive upward. If the particle direction cosine, x, is

$$x = z/\left(\rho^2 + z^2\right)^{1/2} ,$$

then the probability density function (pdf), which describes an isotropic source angular distribution, is

$$p(x) = 1/2, \quad -1 \leq x \leq 1 .$$

A suitable anisotropic pdf, which biases the selection toward certain target direction cosines x_i, is

$$p(x) = A \sum_{i=1}^{N} \left\{1 + \beta_i/\left[1 + \beta_i\left(x - x_i\right)^2\right]\right\} ,$$

where A normalizes p(x) to have an integral of unity (taken from x = -1 to x = 1) and where β_i and x_i are N bias strengths and bias directions. If a β_i is zero, there is no bias toward the corresponding x_i; if all β_i are zero, the pdf is isotropic. The associated cdf is

$$c(x) = \int_{-1}^{x} p(x') \, dx' .$$

and the scattering direction is obtained in the usual way by selecting a random number, ξ, from the uniform distribution on (0,1) and then solving

$$c(x) = \xi$$

for x. The associated weight is simply 1/p(x).

The transport to the first collision was included as part of the source biasing and treated separately from subsequent transport biasing. In addition to the directional biasing already described, two types of path length biasing were used: (1) the well-known exponential transform and (2) an importance function. The exponential transform is not described further since it is a standard technique. For the importance function, instead of sampling from a simple exponential distribution, $e^{-\alpha r}$, in the transport integral

$$\int S e^{-\alpha r} \, dp \ ,$$

where α is the range attenuation coefficient, we wish to sample from the distribution

$$(1 + \gamma r) e^{-\eta r} \ ,$$

where γ is an additional parameter and η is a different attenuation coefficient. Typically, η may be an order of magnitude smaller than α to achieve deep penetration by the first scatter, and γ may be about unity. If γ is zero, the importance function reduces to the exponential transform, while if γ is about unity, the deep penetration statistics are markedly improved over the simple exponential transform. Since gamma ray buildup factors are roughly proportional to r, the γr factor actually suffices to compensate for $1/r^2$ geometric attenuation. A rejection method also was used to eliminate escapes before the first collision.

2.2.2 Transport Biasing

Several methods of biasing the transport kernel were used. A directional exponential transform was sometimes used to force longer transports in the outer direction, but was found unnecessary when region weight balancing and region importances were used with splitting and roulette.

Weight balancing involved keeping the particle weights near an optimum weight, which was a function of the distance from the burst. As necessary, particle weights were adjusted after each collision by splitting or playing roulette. Keeping the weights nearly the same within a volume detector caused the mean square weight to be close to the mean weight, leading to improved statistics. The optimum weight was the first collision weight multiplied by the approximate buildup factor,

$$w_{opt} = B(r) w_1(r) \ ,$$

where $B(r)$ is the approximate buildup factor at range r from the burst and $w_1(r)$ is the first-collision weight at range r. If no source transport bias were used, weight $w_1(r)$ of a particle undergoing a first

collision at range r would be unity for all r. However, the use of the importance function described in section 2.2.1 causes weight w_1 to be a function of r.

Region importances also were implemented. Various regions were assigned numerical ratings of their importance by the input to the SLEDGE code. For example, detectors near the ground were more important than detectors far above the ground. When a particle passed from a region of less importance to a region of greater importance, it was split. When passing the other way, roulette was played. Thus, more particles were tracked in more important regions, and fewer were tracked in less important regions.

2.2.3 Collision Biasing

In several problems, it was found helpful to use collision biasing, in which the emergent particle direction (scattering direction) was biased toward one or more areas of particular interest. The scattering direction was biased only for Compton scattering. For photoabsorption, the gamma ray is completely absorbed. For pair production, the scattering directions of the two locally produced annihilation quanta were assumed to be isotropic and opposite to each other. For Compton scattering, the bias importance function used was

$$I_C = \sum_{i=1}^{M} 1/\left[1 - \kappa_i\left(\hat{r}\cdot\hat{r}_i\right)\right] ,$$

where

κ_i is the bias strength in the ith bias direction,

$\hat{r}$ is the unit vector in the scattering direction,

$\hat{r}_i$ is the unit vector in the ith bias direction.

The dot product $\hat{r}\cdot\hat{r}_i$ is the cosine of the angle between $\hat{r}$ and $\hat{r}_i$ so that I_C is maximized when $\hat{r}$ and $\hat{r}_i$ are parallel.

Construction of a properly normalized pdf based on importance function I_C can be awkward, because the complete angular integral,

$$Q = \int_{4\pi} d\Omega \; I_C \sigma_C(\phi,\theta) ,$$

is required, where $\sigma_C(\phi,\theta)$ is the Compton differential scattering cross section. Since $\sigma_C(\phi,\theta)$ is not a simple function, the integral cannot be obtained analytically. A numerical integration would be time-consuming. Even a straightforward rejection method requires the same

integral to conserve particle weight. Hence, a special algorithm was devised to allow use of the rejection method to implement I_c. The algorithm uses recursive binary splitting with roulette to obtain exactly one surviving particle. The algorithm conserves weight and has a low variance. Briefly, the algorithm consists of the following steps to obtain the biased scattering direction, Ω, for a particle of weight, W:

(1) Select roulette variable V uniformly from the set (1,2).

(2) Generate random trial scattering direction Ω_1 for a first split and get rejection probability R_1.

(3) Test for rejection of the first split. If it is rejected, set $W = W/2$ and return to step (2).

(4) Otherwise, generate random trial scattering direction Ω_2 for a second split and get rejection probability R_2.

(5) Test for rejection of the second split. If it is rejected, set $W = W/(2 - 2/R_1)$, set $\Omega = \Omega_1$, and go to Finish.

(6) Otherwise, if $V = 1$, set $W = W/(1 - R_1)$, set $\Omega = \Omega_1$, and go to Finish.

(7) Otherwise, if $V = 2$, set $W = W/(1 - R_2)$, set $\Omega = \Omega_2$, and go to Finish.

Finish This is the end of the algorithm.

This algorithm allows the use of the rejection method without the need to evaluate normalization integral Q.

In a number of SLEDGE runs, this algorithm was successfully used to push particles away from the ground and toward certain volume detectors with poor statistics.

2.3 Cross Sections

The well-known Klein-Nishina expressions were used for the Compton scattering cross section. For the media under consideration (air and ground), the Compton cross section dominates cross sections for photoabsorption and pair production over a wide energy range.

The attenuation coefficient for pair production was approximated by the simple expression

$$\tau_{pp} \approx 1.84 \times 10^{-4} \rho \bar{Z}^2 \left(\hat{E} - 0.014\hat{E}^2\right)/\bar{A},$$

where

τ_{pp} is in inverse centimeters,

ρ is the material density in grams per cubic centimeter,

$\bar{Z}^2$ is the mean square atomic number of the material,

$\hat{E}$ is E - 1.022, and E is the gamma ray energy in MeV,

$\bar{A}$ is the mean atomic weight of the material.

For air, $\bar{Z}^2 = 106.4$ and $\bar{A} = 28.9$.

For aluminum, $\bar{Z}^2 = 13^2$ and $\bar{A} = 27.0$.

The attenuation coefficient for photoabsorption was approximated by

$$\tau_{ph} \simeq \frac{1.88 \times 10^{-2} \rho \bar{Z}^4}{\bar{A}(100E)^{3.49-0.0035(\log \bar{Z}^4)^2}} ,$$

where the logarithm is to the base 10. The material mean fourth power of the atomic number is 6.46×10^3 for air and 13^4 for aluminum. This approximation has no significant error for air, but is about 10 percent low for aluminum.

The error incurred in the total absorption cross section by using these approximations appears to be less than 1 percent in air for gamma ray energies from 0.01 to 10 MeV. The error in aluminum is slightly greater for energies less than 0.1 MeV. The values for aluminum are cited here because the air-over-ground transport studies were done over an aluminum ground for simplicity. The gamma ray cross-section properties of aluminum are similar to a typical ground composed of silicon, aluminum, oxygen, and water.

2.4 Scoring EMP Drivers by Correlated Sampling

A particularly useful innovation in the SLEDGE code concerns exploitation of the correlation between the energy deposition response function and the (Compton and photoelectric) electron current response function. When EMP drivers are scored, the electron current contribution is found to be correlated with the associated energy deposition contribution. The correlation is high at early times when the gamma ray direction is well collimated, but becomes low at later times when the gamma ray direction is poorly collimated. Ultimately, the correlation drops to zero as the many scatters produce an isotropic gamma direction. The correlation can be exploited in the following way.

Define the energy deposition score in a volume detector, k, and time bin, ℓ,

$$S_{k\ell} = \frac{1}{n} \sum_{m=1}^{n} s_{k\ell m}$$

and the radial (for example) electron current as

$$J_{k\ell} = \frac{1}{n} \sum_{m=1}^{n} j_{k\ell m} ,$$

where m denotes the batch number of a total of n batches. Thus, $s_{k\ell m}$ is the energy deposition score for the kth detector, ℓth time bin, and mth batch. Define also arbitrary function $H_{k\ell}$, which depends on the detector and the time bin. Consider the variance of the linear combination $J_{k\ell} - H_{k\ell}S_{k\ell}$:

$$\text{VAR}\left\{J_{k\ell} - H_{k\ell}S_{k\ell}\right\} = \sum_{m} j^2_{k\ell m} - 2H_{k\ell} \sum_{m} j_{k\ell m}s_{k\ell m} + H^2{}_{k\ell} \sum_{m} s^2_{k\ell m} \quad .$$

If $j_{k\ell m}$ and $H_{k\ell}s_{k\ell m}$ are positively correlated, the negative term on the right hand side reduces the variance; if the correlation coefficient of $j_{k\ell m}$ and $H_{k\ell}s_{k\ell m}$ is unity, the right hand side becomes zero. Therefore, on the assumption that $j_{k\ell m}$ and $H_{k\ell}s_{k\ell m}$ are at least partly correlated, solve the equation

$$j_{k\ell m} = H_{k\ell}s_{k\ell m}$$

for $H_{k\ell}$ by least-squares regression. This regression value for $H_{k\ell}$ should minimize

$$\text{VAR}\left\{J_{k\ell} - H_{k\ell}S_{k\ell}\right\}$$

and make optimum use of any correlation between $j_{k\ell m}$ and $H_{k\ell}s_{k\ell m}$.

In practice with the SLEDGE code, this correlated sampling technique improved the electron radial current fractional deviation statistics by more than an order of magnitude, except at later times when all remaining gamma rays have been scattered many times. The electron theta current statistics were similarly improved by more than a factor of two, *especially* at late times when significant theta currents were developing.

3. CALCULATIONS PERFORMED

3.1 One-Dimensional Studies

The principal aspects of gamma ray transport can be described in terms of buildup factors. (A buildup factor for an effect is the ratio of the effect as engendered by uncollided and multiply scattered gamma ray flux, to the effect as engendered by uncollided gamma flux.) The SLEDGE code was run for seven discrete gamma ray energy sources (table 1) in a homogeneous free air geometry. Results for the time integrated energy deposition buildup factor were obtained from 25 1-d radial bins, each 1 attenuation length wide, extending to a maximum range of 25 attenuation lengths. Fractional deviations varied from about 3 percent at the closer radial bins to about 10 percent for the most distant. For each gamma ray energy, a SLEDGE run was made consisting of 25 batches of 4000 histories each, for a total of 100,000 histories. A typical run tallied about one million collisions (scatters) and consumed about 40 min of central processing unit (CPU) time on the HDL computer (an IBM 370/168). Results were stored on magnetic tape for subsequent analysis and curve fitting.

TABLE 1. SEVEN GAMMA RAY ENERGIES AND ATTENUATION PARAMETERS

Source gamma ray energy (MeV)	Total attenuation coefficient (m^{-1})	1 attenuation length (m)	25 attenuation lengths (m)
0.5	0.009604	104.12	2603.08
1.0	0.007014	142.57	3564.30
1.5	0.005734	174.40	4359.96
2.5	0.004377	228.47	5711.67
3.5	0.003651	273.90	6847.44
5.0	0.003034	329.60	8239.95
7.0	0.002596	385.21	9630.20

Table 1 lists the total attenuation coefficient and distances corresponding to 1 and 25 attenuation lengths. An air density of 1.11 × kg/m^3 is assumed.

Time-dependent results also were obtained from these studies. The time bin structure used was the same as for the 2-d problems, shown in table 2.

TABLE 2. SLEDGE MESHES FOR TWO-DIMENSIONAL PROBLEMS

Time bin boundaries (s)	Radial boundaries (m)	Vertical boundaries (m)
0.00	0.0	-1.0
5.00(-9)[a]	300.0	0.0[b]
1.00(-8)	600.0	25.0
2.00(-8)	900.0	50.0
3.25(-8)	1200.0	100.0
5.00(-8)	1500.0	200.0
7.50(-8)	1800.0	400.0
1.00(-7)	2100.0	600.0
1.50(-7)	2400.0	3000.0
2.00(-7)	2700.0	
3.00(-7)	3000.0	
4.00(-7)		
6.00(-7)		
1.00(-6)		
1.50(-6)		
2.00(-6)		
3.00(-6)		
5.00(-6)		
1.00(-5)		

[a] *Read as* 5.00×10^{-9}.

[b] *Air-ground interface at 0.0-m height.*

3.2 Two-Dimensional Air-Ground Interface Effects

The 2-d air-over-ground gamma ray transport problem may be considered as a perturbed free-field problem. Significant perturbations are expected near the air-ground interface. The SLEDGE code was run for a 1.5-MeV gamma ray source in a cylindrical air-over-ground geometry. A burst height of 200 m was used. As mentioned in section 2.3, the ground was assumed for simplicity to be aluminum, whose gamma ray cross-section

properties are analogous to a typical ground composed of silicon, aluminum, oxygen, and water. The radial (horizontal) mesh extended to a 3000-m ground range, and the vertical mesh extended to a 3000-m height aboveground and to a 1-m depth belowground. Eighteen time bins were used, extending to a 10-μs retarded time. These grids are shown in table 2. Correlated sampling was used for the radial Compton current, but not for the theta Compton current. Various biases and importance functions were used, as described in section 2.2. The run consisted of 30 batches of 20,000 histories each, for a total of 600,000 histories. In longer than 2 hr of CPU running, nearly four million collisions (scatters) were tallied. Fractional deviations for energy deposition averaged 1 percent close to the burst and about 6 percent near the 3-km boundary.

It was observed that energy deposition from outgoing gamma rays was about eight times that from backscattered incoming gamma rays, at any range in the air. The backscatter from the ground was much less, so that radial Compton current and energy deposition were weaker near the ground and the theta Compton current was strongest. This effect is clear since gamma rays must flow from the air into the ground and be attenuated there; this flow causes a negative gradient in the flux close to the ground. From a different viewpoint, the buildup factor is reduced near the ground.

Since effects due to multiply scattered gamma rays come later in time than effects due to unscattered gamma rays, the time dependence of effects was confirmed to be range dependent. At deeper penetrations, the buildup factor is greater so that multiply scattered effects are stronger. The result is that the energy deposition decay rate in time is slower at deeper penetrations. The ratio of radial Compton current to energy deposition rate also declines with time more slowly with increasing range. In fact, the time dependence of the latter ratio roughly scales as the inverse of the buildup factor (that is, scaled time $t' \approx tB$).

A similar SLEDGE run was done for a 0.5-MeV gamma ray source. Results of both runs were stored on magnetic tape for subsequent analysis.

PART II. ANALYTICAL FITS TO EMP DRIVER RESULTS

4. ENERGY DEPOSITION

4.1 Fitting Free-Field Buildup Factors for Seven Gamma Ray Energies

Seven gamma ray energies from 0.5 to 7.0 MeV (table 1) were chosen to allow flexibility in representing approximately an arbitrary nuclear burst gamma ray energy spectrum. Since gamma-induced EMP sources may contribute to EMP generation at distances as great as about 5 km, the gamma ray transport was carried to a range of 25 attenuation lengths to ascertain the true range dependence of the buildup factor for energy deposition. Based on theory, a reasonable approximation to the buildup factor is given by

$$B(r) = 1 + a(r/\lambda)^k ,$$

where λ is the attenuation length and a may be shown by energy conservation to be

$$a = \mu_s/[\mu_a \Gamma(k+1)] ,$$

where

μ_s = total scattering coefficient ($\mu_s = \sigma_s + 1.022\sigma_{pp}/E$),

σ_s = Compton scattering coefficient,

σ_{pp} = pair production attenuation coefficient,

E = gamma ray energy in MeV,

μ_a = total absorption coefficient for Compton absorption, photoabsorption, and pair production $[\mu_a = \sigma_a + \sigma_{ph} + \sigma_{pp}(E - 1.022)/E]$,

σ_a = Compton absorption coefficient,

σ_{ph} = photoabsorption attenuation coefficient,

$\Gamma(k+1)$ = gamma function of $k+1$,

k = function of (source) gamma ray energy.

Parameter k is of order unity and is the only free quantity in the expression for B.

The expression for B was fitted, by adjustment of k, to the 1-d detector results obtained by the SLEDGE code. Twenty-five detectors were used, each one attenuation length thick. The least-squares fit was

obtained by minimizing the sum of the squares of the errors over all detectors, with each square weighted by the reciprocal of the square of the fractional deviation for the detector. Buildup factor parameters a and k so obtained are given in table 3 for each gamma ray energy. The buildup factor predicted by these values of a and k has a probable error of not more than 1 percent due to the uncertainty in the Monte Carlo data. Although the fractional deviation for the detectors varies from about 3 to about 10 percent, the combined fractional deviation (of all 25 detectors fitted at once) is less than 1 percent. However, this 1-percent error estimate does not include the possibility of systematic error due to the true buildup factor not being perfectly represented by the expression $1 + a(r/\lambda)^k$. This error estimate does describe how closely the a and k parameter values, thus obtained by fitting Monte Carlo data, approximate the *best fit* of the expression to the true buildup factor.

TABLE 3. ENERGY DEPOSITION BUILDUP FACTOR PARAMETERS FOR $B = 1 + a(r/\lambda)^k$

Source gamma ray energy (MeV)	a	k
0.5	1.534	1.418
1.0	1.162	1.188
1.5	0.960	1.143
2.5	0.800	0.976
3.5	0.695	0.903
5.0	0.580	0.880
7.0	0.473	0.891

As to possible systematic error, it appears that the fit may be low by about an average 2 percent to 10 attenuation lengths range, but this level remains uncertain because of the size of statistical error of the Monte Carlo data. Statistical error at farther ranges is even greater and permits no assessment of systematic error.

4.2 Ground Effect on Buildup Factor

Analysis of the 2-d detector results of the two SLEDGE runs, for 0.5- and 1.5-MeV gamma ray point sources at 200 m aboveground, showed a distinct depletion of energy deposition near the ground. An exception is that early energy deposition is enhanced beneath the burst due to immediate backscatter from the ground. However, this effect will be neglected in the following development since EMP in this region is not important to typical Army electronic systems because of overwhelming blast and thermal damage.

For observers near the ground and for a range such that the line of sight to the burst is shallow, the buildup factor was limited in its growth. This limitation was interpreted that the ground (although

flat) introduced an effective horizon because the ground intercepts multiply scattered gamma rays that would otherwise contribute. The effective horizon, H, is approximately

$$H = 3.0r/\left(9.0 + r^2/\lambda^2\right)^{1/2}$$

for horizontal gamma ray incidence near the ground.

The effective horizon for horizontal incidence, h, at height z aboveground is approximately

$$h = He^{z/\lambda} .$$

For incidence at angle θ to the horizontal, the effective horizon at the observer will be approximated by the averaging integral

$$h = \int_0^H e^{z(r)/\lambda}\, dr = \int_0^H e^{[r(\sin\theta)+Z]/\lambda}\, dr ,$$

or

$$h = \frac{\lambda e^{Z/\lambda}}{\sin\theta}\left[e^{H(\sin\theta)/\lambda} - 1\right] ,$$

where z(r) is the height at range r on the line of sight from the burst to the observer and Z is the observer height aboveground.

The ground-influenced buildup factor, $\hat{B}(R,Z)$, a function of observer range and height, is asymptotically limited to B(h), that attained within effective horizon h. Based on the SLEDGE 2-d results, a good approximation for the ground-influenced buildup factor is

$$\hat{B}(R,Z) = (1/2)[B(r) + X] ,$$

where B(r) is the free-field buildup factor for range r from the source and

$$X = 1 + 1/\left(1/[B(r) - 1]^2 + 1/\left\{4 + [B(h) - 1]^2\right\}\right)^{1/2} .$$

4.3 Time Dependence of Energy Deposition Rate

The time-dependent energy deposition rate, S, at distance r, height z, and time t contributed by multiply scattered gamma rays (that is, excluding uncollided gamma rays) from a delta-function (in time) point gamma source of one gamma of energy, E, is written as

$$S(r,z,t) = U(r)N(r,z)T(r,z,t) ,$$

where

$U(r)$ = energy deposition from uncollided gamma ray *number* flux (that is, first-scatter deposition),

$N(r,z)$ = normalization factor (including buildup factor),

$T(r,z,t)$ = explicit time dependence.

$U(r)$ is given by

$$U(r) = Ee^{-r/\lambda} / \left(4\pi r^2 \lambda_{abs}\right) ,$$

where E is the gamma ray energy, λ is the attenuation length, and λ_{abs} is the absorption length. Based on the 1.5-MeV gamma ray source SLEDGE results, a good approximation for T is

$$T(r,z,t) = \left(t + t_0\right)^m e^{-pt} ,$$

where

$t_0 = 10^8$ s,

$m = -1/[1 + f(r,z)r/\lambda]$,

$p = 1.4 \times 10^6$ s^{-1}.

Function $f(r,z)$ is described later.

We require S to be independent of z at $t = 0$ since the ground affects only multiply scattered gamma rays (for an observer above-ground), and these gamma rays always arrive after $t = 0$. We require also the following normalization:

$$\int_0^\infty S(r,z,t)\, dt = U(r)\left[\hat{B}(r,z) - 1\right] ,$$

where $\hat{B}$ is the ground-influenced buildup factor. For $z = \infty$, $\hat{B}$ becomes free-field buildup factor $B(r)$. From this normalization, we obtain

$$N(r,z) \int_0^\infty T(r,z,t)\, dt = \hat{B}(r,z) - 1 .$$

Let I be defined as the integral

$$I = \int_0^\infty T(r,z,t)\, dt$$

$$= \int_0^\infty \left(t + t_0\right)^m e^{-pt}\, dt .$$

By straightforward means, the integral is found to be

$$I = e^{pt_0} p^{-\varepsilon} \Gamma(\varepsilon)\left[1 - P(\varepsilon, pt_0)\right] ,$$

where

ε = $1 + m$,

$\Gamma(\varepsilon)$ = gamma function of ε,

$P(\varepsilon, pt_0)$ = incomplete gamma function.[5]

Hence, normalization factor $N(r,z)$ is

$$N(r,z) = \left[\hat{B}(r,z) - 1\right]/I .$$

Since function $f(r,z)$ has not been specified yet, variable ε,

$$\varepsilon = 1 - 1/[1 + f(r,z)r/\lambda] ,$$

remains unconstrained. We use it to satisfy the requirement that $S(r,z,t)$ be independent of z at $t = 0$. At earliest times, the transport is essentially free field, so free-field data far from the ground should describe the $t = 0$ transport. By examination of SLEDGE data for detectors far from the ground (virtually free field), it was determined that a value $f = 0.2$ would cause S to fit these data reasonably well. This value is called f_∞ (that is, $f_\infty \equiv 0.2$). Let the corresponding value for ε be

$$\varepsilon_\infty = 1 - 1/\left(1 + f_\infty r/\lambda\right) .$$

We require the transport near the ground at $t = 0$, to be the same as the transport far ($z \to \infty$) from the ground, also at $t = 0$. Thus,

$$S(r, z=\infty, t=0) \equiv S(r,z,t=0) ,$$

or

$$\frac{[B(r) - 1]T(r, z=\infty, t=0)}{I(r, z=\infty)} = \frac{\left[\hat{B}(r,z) - 1\right]T(r,z,t=0)}{I(r,z)} .$$

This can be expanded to

$$\frac{[B(r) - 1]t_0^{\varepsilon_\infty - 1}}{e^{pt_0} p^{-\varepsilon_\infty}\Gamma(\varepsilon_\infty)\left[1 - P(\varepsilon_\infty, pt_0)\right]} = \frac{\left[\hat{B}(r,z) - 1\right]t_0^{\varepsilon - 1}}{e^{pt_0} p^{-\varepsilon}\Gamma(\varepsilon)\left[1 - P(\varepsilon, pt_0)\right]} ,$$

[5] *Milton Abramowitz and Irene Stegun, Handbook of Mathematical Functions, Dover Publications, Inc., New York (1965), 260.*

where ε is a function of z. If we define $G(\varepsilon)$ by

$$G(\varepsilon) = t_0^{1-\varepsilon} e^{pt_0} p^{-\varepsilon} \Gamma(\varepsilon)\left[1 - P(\varepsilon, pt_0)\right] ,$$

then this may be written

$$[B(r) - 1]/G(\varepsilon_\infty) = \left[\hat{B}(r,z) - 1\right]/G(\varepsilon)] ,$$

or

$$G(\varepsilon) = G(\varepsilon_\infty)\left[\hat{B}(r,z) - 1\right]/[B(r) - 1] .$$

Thus, given r and z, $G(\varepsilon)$ may be determined from $G(\varepsilon_\infty)$, $B(r)$, and $\hat{B}(r,z)$. $G(\varepsilon)$ may then be inverted to yield ε. Having ε and $m = \varepsilon - 1$, one may obtain

$$I = G(\varepsilon) t_0^m ,$$

$$N(r,z) = \left[\hat{B}(r,z) - 1\right]/I ,$$

$$T(r,z,t) = (t + t_0)^m e^{-pt} ,$$

$$S(r,z,t) = U(r)N(r,z)T(r,z,t) .$$

Inverting $G(\varepsilon)$ for ε involves tabulating G for a large number of values of ε and then using a table-lookup algorithm to get ε from G.

By using the approach just described, the energy deposition rate may be obtained for any r,z,t in such a way that it evolves in time from an initial free-field distribution to a progressively more ground-influenced distribution. Time integrals of the energy deposition rate are correctly normalized to expected ground-influenced buildup factors.

These results are scaled to first order to source gamma ray energies other than 1.5 MeV by geometrically scaling r, z, and t by the attenuation length. This is already built into buildup factors B and $\hat{B}$ and variable m (and ε). Only the time remains to be scaled. If subscript "1.5" denotes 1.5-MeV source gamma rays and if

$$\alpha \equiv \lambda_{1.5}/\lambda(E) ,$$

where $\lambda(E)$ is the attenuation length for gamma ray energy E, then

$$G(\varepsilon) = (\alpha t_0)^{1-\varepsilon} e^{p\alpha t_0} p^{-\varepsilon} \Gamma(\varepsilon)\left[1 - P(\varepsilon, p\alpha t_0)\right] ,$$

$$I = G(\varepsilon)(\alpha t_0)^m/\alpha ,$$

$$T(r,z,t) = (\alpha t + \alpha t_0)^m e^{-p\alpha t} .$$

Variable m is evaluated for $\lambda = \lambda(E)$ as

$$m = - 1/[1 + fr/\lambda(E)] \ .$$

The uncollided energy deposition, U, becomes

$$U(r) = Ee^{-r/\lambda(E)}/[4\pi r^2 \lambda_{abs}(E)] \ .$$

5. RELATION OF COMPTON CURRENT TO ENERGY DEPOSITION RATE

5.1 Compton Current from First Collisions of Gamma Rays

For point source gamma rays experiencing their first collision in air having density 1.11 kg/m^3, the radial Compton current produced is simply related to the corresponding energy deposition:

$$J_r/S = k_0(E) \ .$$

The theta Compton current, J_θ, is identically zero for first scatters. Factor $k_0(E)$ is given in table 4 for the seven gamma ray energies considered. The values are based on estimates[6] of the mean forward range of Compton electrons, including multiple scattering of the Compton electrons as well. Factor $k_0(E)$ equals $\lambda_a R_c/(\rho \lambda_c E)$, where λ_a and λ_c are the Compton absorption and collision lengths, ρ is the air density, R_c is the mean forward range of the Compton electrons, and E is the gamma ray energy.

TABLE 4. RATIO OF RADIAL COMPTON ELECTRON CURRENT TO ENERGY DEPOSITION FOR FIRST-COLLISION GAMMA RAYS FROM A POINT SOURCE

Source gamma ray energy (MeV)	Ratio $k_0(E)$ (electron-m/MeV)
0.5	1.061
1.0	1.606
1.5	1.952
2.5	2.338
3.5	2.508
5.0	2.561
7.0	2.454

[6] *William T. Wyatt, Jr., Transmission Factor Effects on the Average Forward Range of Compton Electrons, Harry Diamond Laboratories HDL-TM-80-10 (January 1980).*

5.2 Radial Compton Current from Multiply Scattered Gamma Rays

For multiply scattered gamma rays, the radial Compton current produced is related to the corresponding energy deposition by

$$J_r/S = k(r,t,E) ,$$

where r is the distance from the point source of gamma rays and t is retarded time. The SLEDGE 1-d results for each of the seven gamma ray energies can be fitted by

$$k(r,t,E) \approx k_0(E)\left(0.91 + 0.03E^{1/2}\right)e^{-T} ,$$

where

$$T = \frac{1.0 \times 10^{-8} p_1 \left(1.0 \times 10^{8} t\right)^{p_2}}{[B(R) - 1]^{p_4}}$$

and

$$R = r + \lambda\left(p_3 + p_5 t/[r/\lambda]^{p_6}\right) .$$

Factor $k_0(E)$ is defined in section 5.1. Buildup factor B is evaluated for modified range R. Optimum fit values for p_1, p_2, p_3, p_4, p_5, and p_6 are listed in table 5 for the seven gamma ray energies.

TABLE 5. FIT PARAMETERS FOR RATIO OF RADIAL COMPTON ELECTRON CURRENT TO ENERGY DEPOSITION RATE FOR MULTIPLY SCATTERED GAMMA RAYS

Source gamma ray energy (MeV)	p_1	p_2	p_3	p_4	p_5	p_6
0.5	3.880(7)[a]	1.384	7.599(-2)	0.855	2.793(7)	-0.0847
1.0	1.783(7)	1.040	1.304(-1)	0.685	0.817(7)	+0.0524
1.5	1.162(7)	1.025	7.358(-2)	0.596	0.537(7)	-0.1179
2.5	0.964(7)	0.974	1.765(-2)	0.679	0.339(7)	+0.0605
3.5	0.769(7)	0.974	1.679(-2)	0.758	0.247(7)	+0.1410
5.0	0.358(7)	1.230	7.253(-2)	0.947	0.523(7)	-0.1091
7.0	0.835(6)	1.865	7.869(-2)	1.561	1.336(7)	-0.0886

[a] *Read as* 3.880×10^7.

Quantity k(r,t,E) decays more slowly with increasing range. Also, in theory one would expect k at time t = 0 to be exactly $k_0(E)$ since the earliest scattered gamma rays to arrive at any point are those that have experienced a single grazing scatter and thus have nearly the same energy, E. However, the Monte Carlo studies show that

$$k(r,t,E) \approx k_0(E)\left(0.91 + 0.03E^{1/2}\right)$$

when averaged over the first time bin, which is 5 ns wide. This resolution of the time history appears to be adequate since most gamma ray output from a nuclear burst is emitted over about 10 ns.

5.3 Theta Compton Current from Multiply Scattered Gamma Rays

The theta Compton current from a point gamma ray source near the earth is secondary to the radial Compton current in magnitude and in efficiency as a generator of EMP. In the SLEDGE 2-d results, variance was larger for the theta current component--often so large that the sign of the component was doubtful. Nevertheless, some significant trends were clearly observed at late times near the ground. The ratio of theta Compton current to energy deposition rate (for an air density of 1.11 kg/m^3) is approximately

$$J_\theta/S = 1.5 \times 10^5 te^{-0.02z} ,$$

where t is retarded time in seconds and z is height aboveground in meters. Thus, the theta component is strongest near the ground and decays (about) exponentially with increasing height.

This expression for J_θ/S is not strongly dependent upon source gamma ray energy to a first approximation since the late-time currents derive from low-energy multiply scattered gamma rays.

6. COMPARISON WITH PREVIOUS RESULTS

6.1 Buildup Factor for Energy Deposition

The LEMP code prompt gamma ray drivers (H. J. Longley, Mission Research Corp.) include buildup factor curve fits for energy deposition and radial Compton current for three source gamma ray energies (0.5, 1.5, and 5.0 MeV). No account is taken of the influence of the ground. The energy deposition buildup factor obtained for air was based on published data for water.

Recently, Malik, Cashwell, and Schrandt[7] at the Los Alamos Scientific Laboratory (LASL) obtained curve fits to buildup factors and

[7] *J. S. Malik, E. D. Cashwell, and R. G. Schrandt, The Time Dependence of the Compton Current and Energy Deposition from Scattered Gamma Rays, Los Alamos Scientific Laboratory, NM, LA-7386-MS (July 1978).*

time dependence of energy deposition and Compton current from scattered gamma rays in homogeneous isotropic air. These curve fits to their Monte Carlo data were obtained for gamma ray energies of 1, 1.5, 2, 3, 4, and 6 MeV to a range of 1600 m. Air density was 1.1 mg/cm^3.

The LEMP and LASL buildup factors are compared with NEMP free-field and ground-influenced buildup factors (for energy deposition) in figures 1 to 6. The NEMP ground-influenced buildup factor is for a burst and an observer both at a 0-m height aboveground. Figures 1 to 3 show results as a function of range in units of attenuation lengths, from 0 to 25 attenuation lengths. These results exclude the effect of any disagreement in attenuation length among the LEMP, LASL, and NEMP drivers and compare directly the functional forms used. Figures 1 to 3 show, respectively, 0.5-, 1.5-, and 5.0-MeV source gamma ray buildup factors. The 0.5-MeV energy is below the 1.0-MeV lower limit for the LASL transport data and shows that the LASL drivers are in substantial error below the designated range. The LEMP and NEMP curves are in good agreement to about four attenuation lengths range, after which the LEMP curve is higher. For 0.5 MeV, the disagreement becomes very large. The quality of agreement between LEMP and NEMP at closer ranges, however, tends to confirm their validity at such ranges. The LASL curves, on the other hand, seem too low except for the 5.0-MeV results (fig. 3). The low-energy disagreement among LEMP, NEMP, and LASL is ameliorated by the fact that, for a realistic gamma ray energy spectrum, higher energy gamma rays predominate at substantial ranges because of their greater penetrating ability.

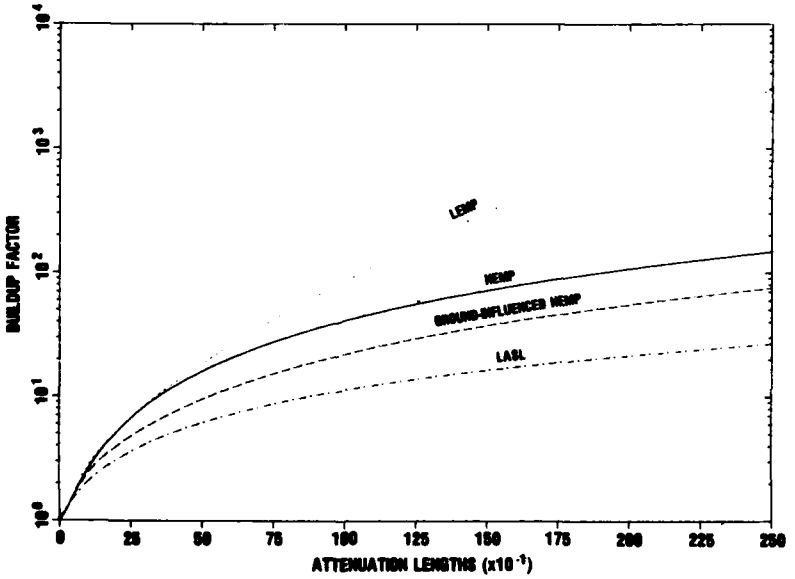

Figure 1. Energy deposition buildup factors compared for 0.5-MeV gamma rays, for range in attenuation lengths.

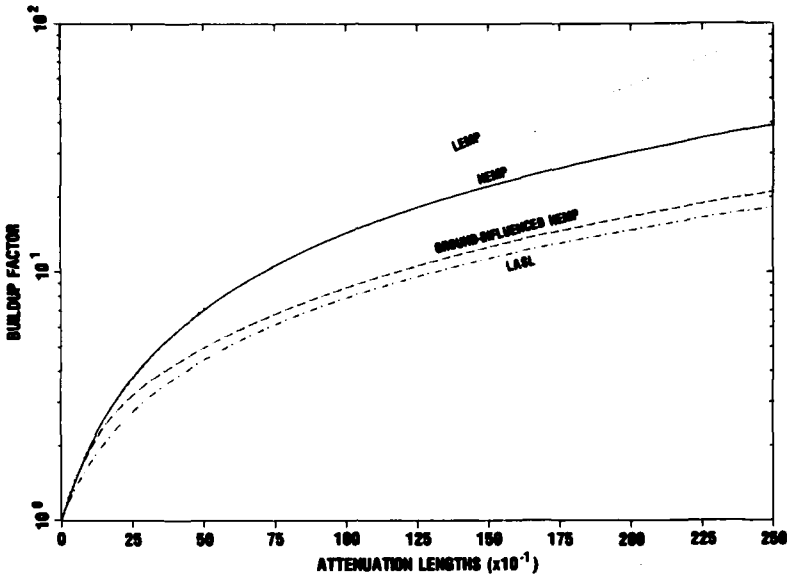

Figure 2. Energy deposition buildup factors compared for 1.5-MeV gamma rays, for range in attenuation lengths.

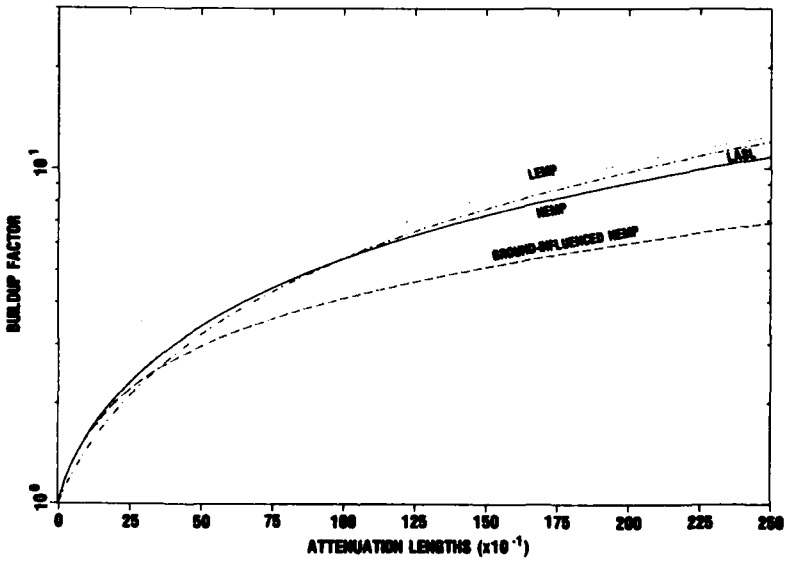

Figure 3. Energy deposition buildup factors compared for 5.0-MeV gamma rays, for range in attenuation lengths.

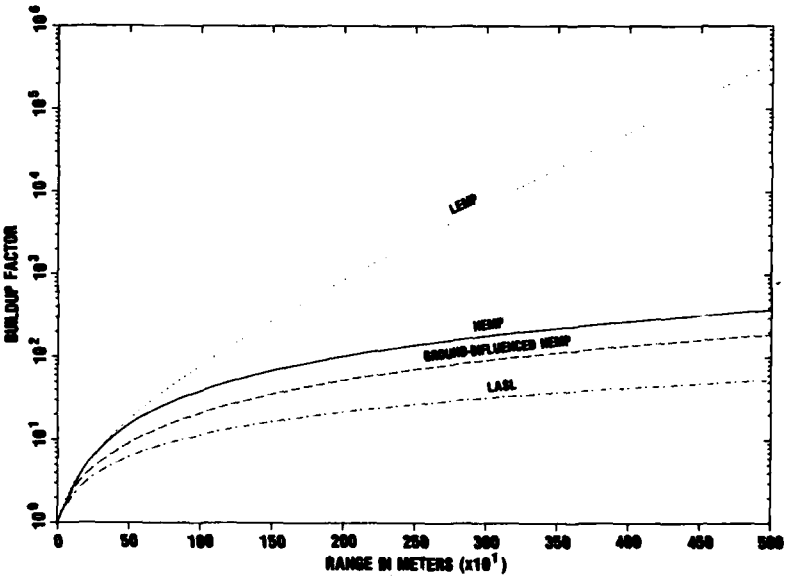

Figure 4. Energy deposition buildup factors compared for 0.5-MeV gamma rays, for range in meters.

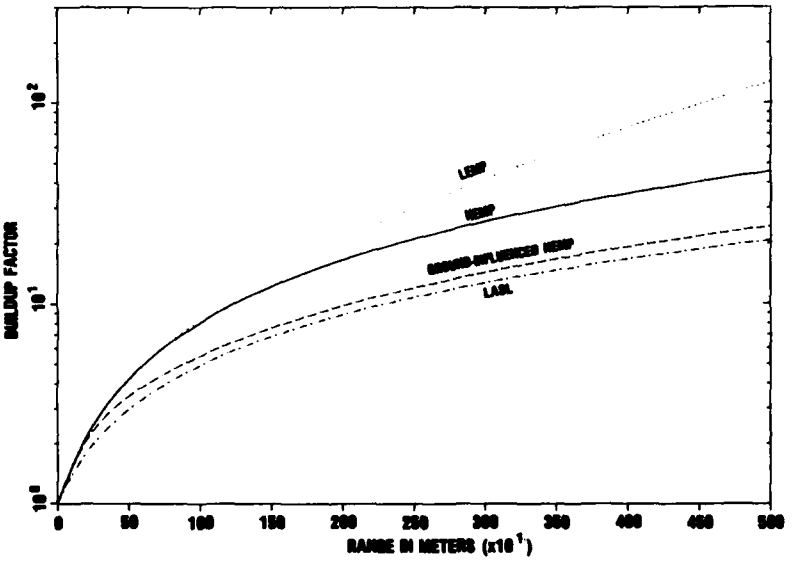

Figure 5. Energy deposition buildup factors compared for 1.5-MeV gamma rays, for range in meters.

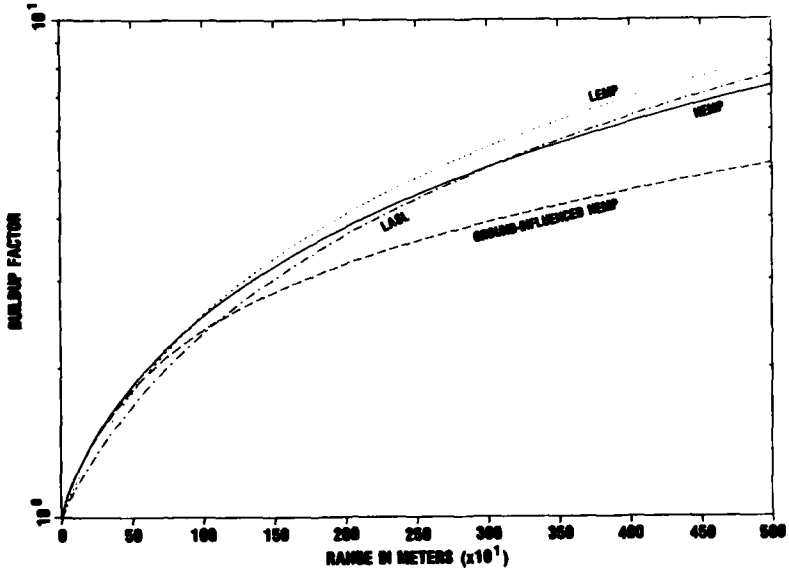

Figure 6. Energy deposition buildup factors compared for 5.0-MeV gamma rays, for range in meters.

Figures 4 to 6 include the attenuation length, but still appear similar to figures 1 to 3. Careful comparison of SLEDGE transport results with the NEMP curve fit shows that the NEMP curve fit is about 10 percent higher over the first attenuation length. But the NEMP curve fit is found to be accurate to a few percent at greater ranges.

The NEMP ground-influenced buildup factor in figures 1 to 6 is as much a factor of two smaller than the corresponding NEMP free-field buildup factor. The difference increases monotonically with range, more slowly for more energetic gamma rays, to a difference of as much as a factor of two.

6.2 Time Dependence of Energy Deposition Rate

The time dependence of the free-field NEMP, LEMP, and LASL energy deposition rate drivers is shown in figures 7 to 12 for three source gamma ray energies (0.5, 1.5, and 5.0 MeV) and two ranges from the burst (300 and 3000 m). The three curves are normalized to a time integral of unity, removing any disagreement in attenuation length and buildup factor. A fourth curve represents the ground-influenced NEMP energy deposition rate for burst and observer on the ground. This curve is normalized to the free-field case, so the difference between this curve and the free-field NEMP curve is a diminution of the energy deposition rate due to the presence of the ground.

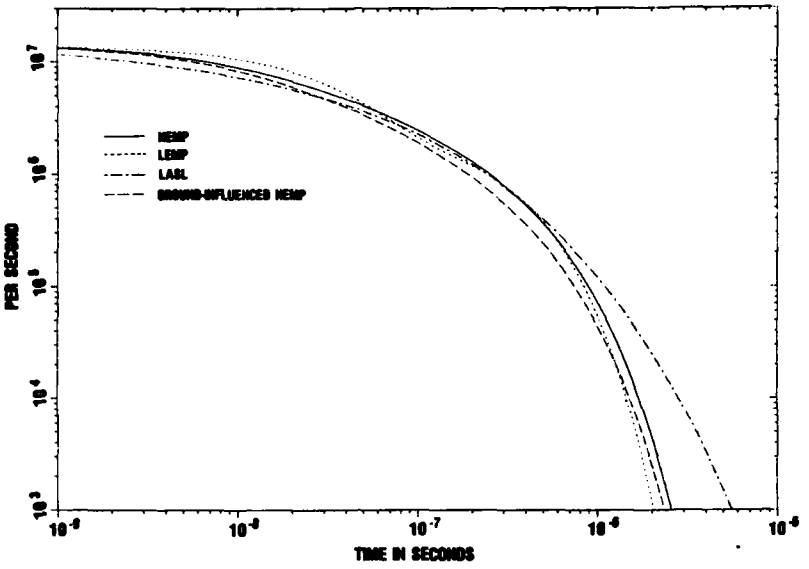

Figure 7. Time dependence of energy deposition buildup factors compared at 300-m range for 0.5-MeV gamma rays.

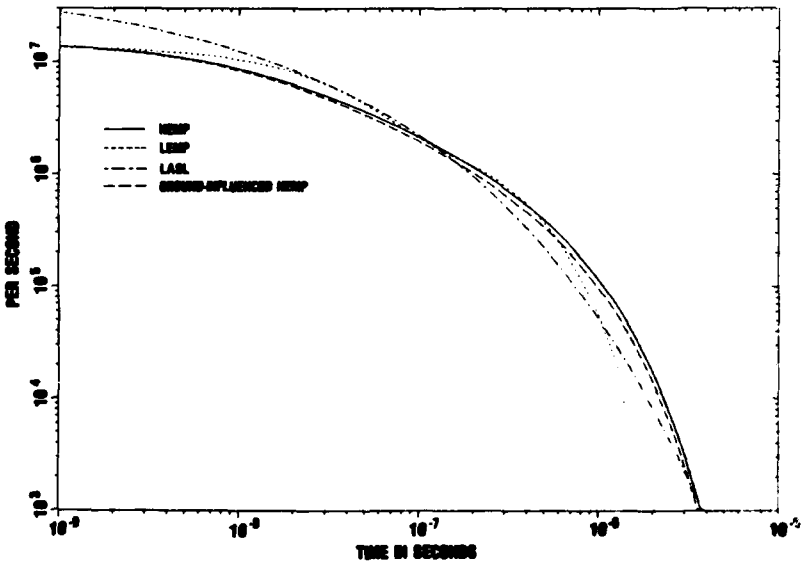

Figure 8. Time dependence of energy deposition buildup factors compared at 300-m range for 1.5-MeV gamma rays.

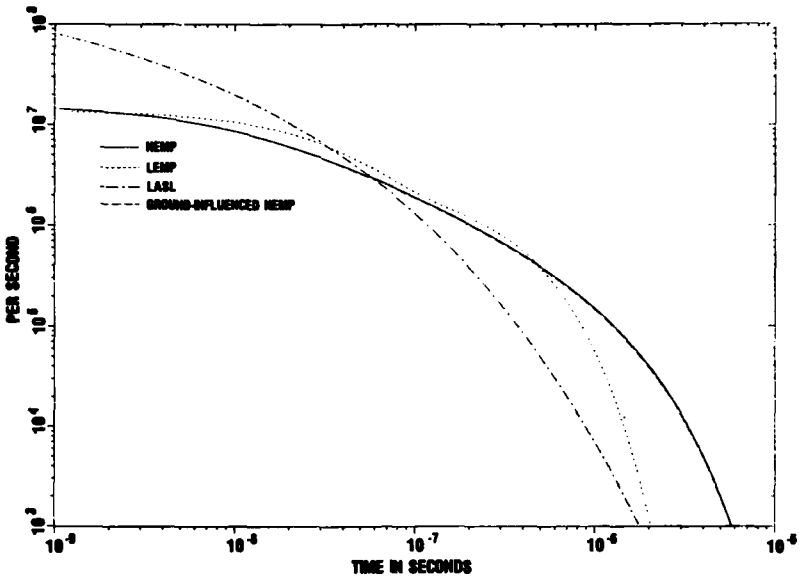

Figure 9. Time dependence of energy deposition buildup factors compared at 300-m range for 5.0-MeV gamma rays.

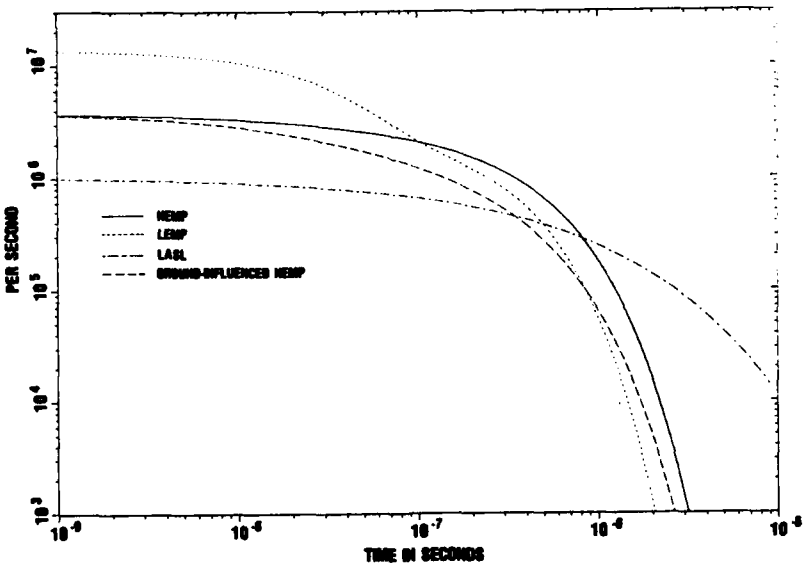

Figure 10. Time dependence of energy deposition buildup factors compared at 3000-m range for 0.5 MeV-gamma rays.

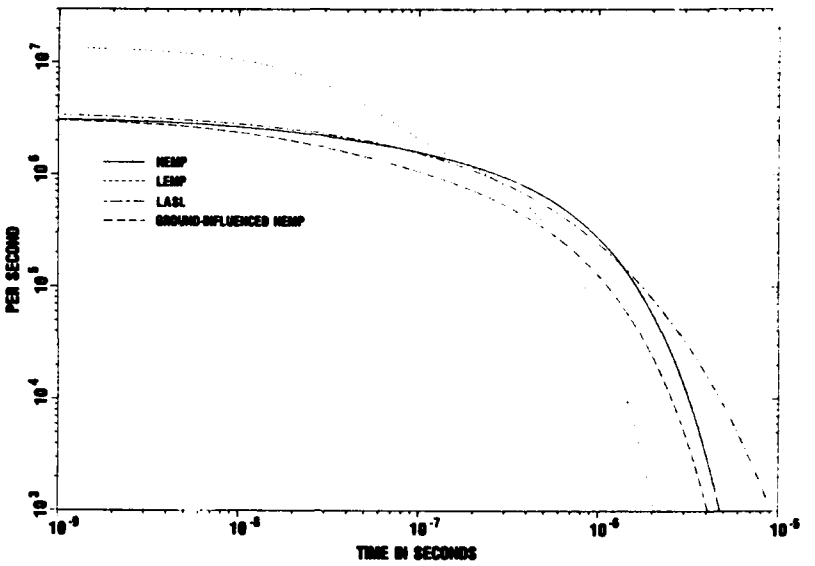

Figure 11. Time dependence of energy deposition buildup factors compared at 3000-m range for 1.5-MeV gamma rays.

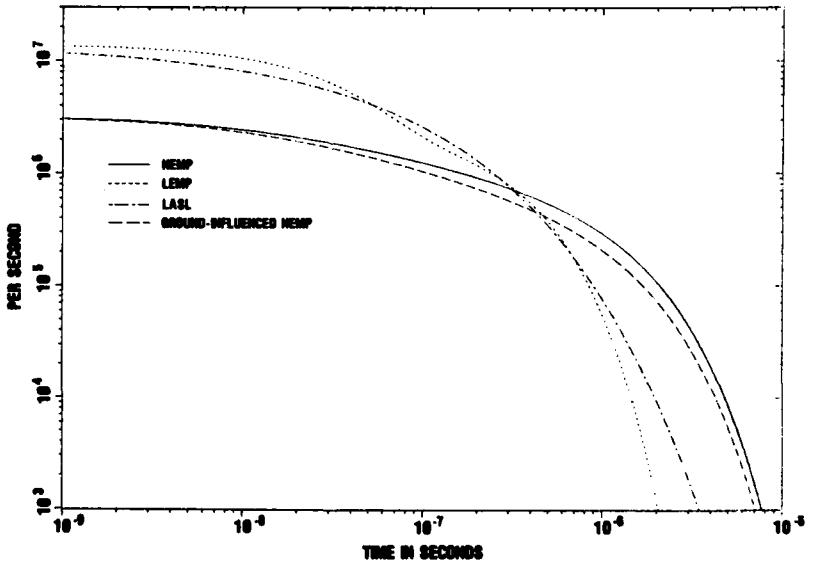

Figure 12. Time dependence of energy deposition buildup factors compared at 3000-m range for 5.0-MeV gamma rays.

Figures 7 to 9 show the energy deposition rate at a 300-m range for 0.5-, 1.5-, and 5.0-MeV source gamma ray energies. The agreement between the NEMP and LEMP drivers is good. Since the LEMP driver was based on close-in data, we expect it to be accurate at a 300-m range. The extremely close agreement at 1-ns retarded time is particularly encouraging and tends to confirm the correctness of the first-scatter part of the NEMP driver. The LASL curve seems to be concentrated too much toward early times, except for the 0.5-MeV curve.

Figures 10 to 12 show the energy deposition rate at a 3000-m range for 0.5-, 1.5-, and 5.0-MeV source gamma ray energies. At this deep penetration, we expect the LEMP curves to be concentrated too much toward early times in comparison with the NEMP curve--and they are. The NEMP and LASL curves agree well only for 1.5 MeV (fig. 11). For 5.0 MeV (fig. 12), the LASL curve is too close to the LEMP curve. Data shown in the LASL report[7] confirm a tendency of that curve fit to overestimate the energy deposition rate earlier than a fraction of a microsecond, for deep penetrations of about 10 attenuation lengths.

In all figures shown, the NEMP ground-influenced energy deposition rate begins equal to the NEMP free-field curve and later falls below by as much as a factor of about three for the 3000-m curve. For the 300-m curve, little difference is noted.

6.3 Time Dependence of Radial Compton Current

The ratio of radial Compton electron current to energy deposition rate is shown as a function of time for the NEMP, LEMP, and LASL drivers in figures 13 to 18. Figures 13 to 15 are for gamma ray energies of 0.5, 1.5, and 5.0 MeV at a range of 300 m from the burst. Figures 16 to 18 are for the same gamma ray energies at a range of 3000 m. The units of the ratios plotted are in Compton electron-meter per MeV. A factor of 0.8 has been separately applied to the LEMP and LASL drivers to account for multiple scattering of Compton electrons. This effect is already included in the NEMP driver. As for energy deposition rate, we expect the LEMP data to be more accurate at 300 m than at 3000 m. Good agreement is observed among all three curves (NEMP, LEMP, and LASL) at 300 m for each gamma ray energy, with a few exceptions. The NEMP curve is probably too high after about 1 μs, although the significance of the discrepancy is slight in terms of the EMP that would be produced. Also, the LASL early time value for 0.5 MeV is high by more than a factor of two.

---

[7] *J. S. Malik, E. D. Cashwell, and R. G. Schrandt, The Time Dependence of the Compton Current and Energy Deposition from Scattered Gamma Rays, Los Alamos Scientific Laboratory, NM, LA-7386-MS (July 1978).*

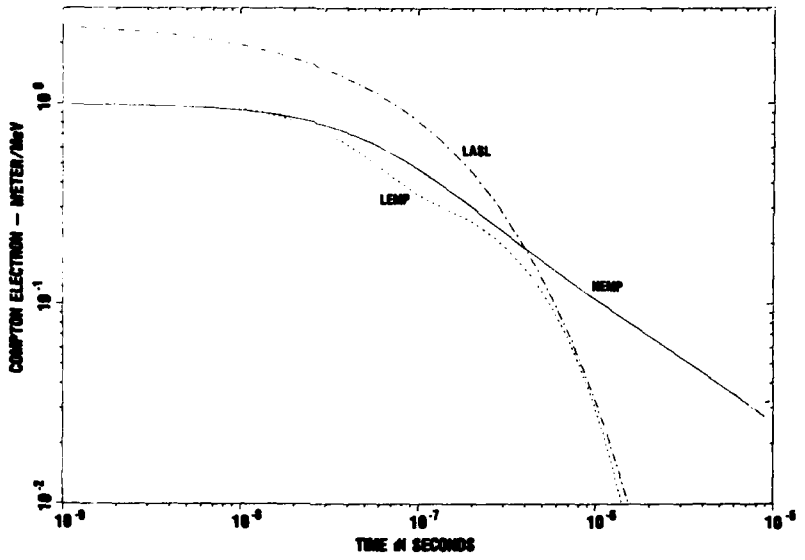

Figure 13. Time dependence compared for ratio of radial Compton electron current to energy deposition rate, at 300-m range for 0.5-MeV gamma rays.

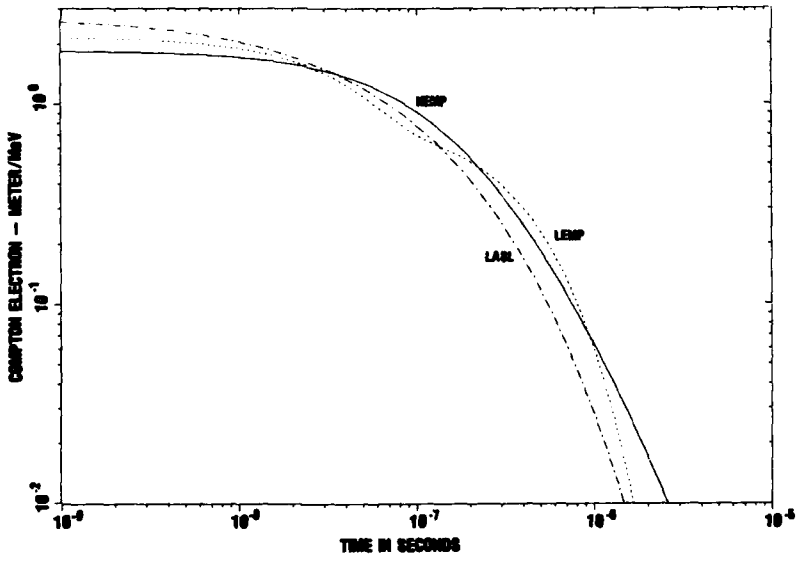

Figure 14. Time dependence compared for ratio of radial Compton electron current to energy deposition rate, at 300-m range for 1.5-MeV gamma rays.

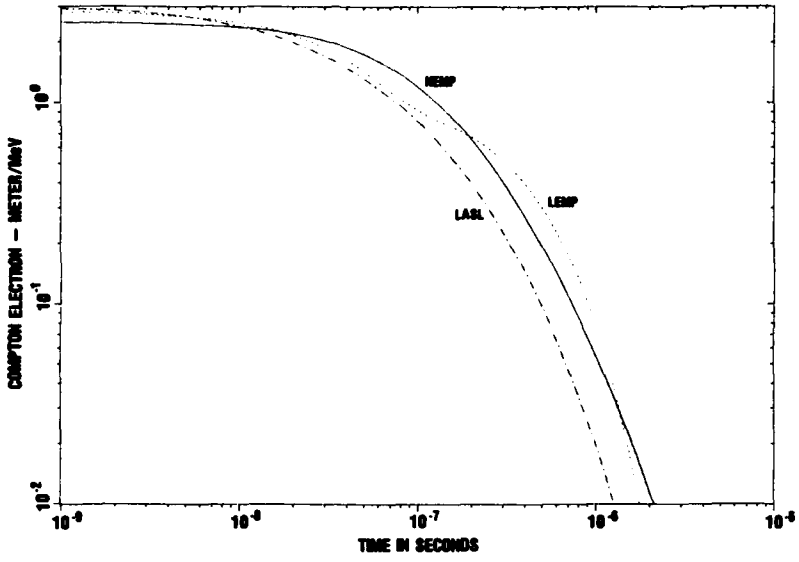

Figure 15. Time dependence compared for ratio of radial Compton electron current to energy deposition rate, at 300-m range for 5.0-MeV gamma rays.

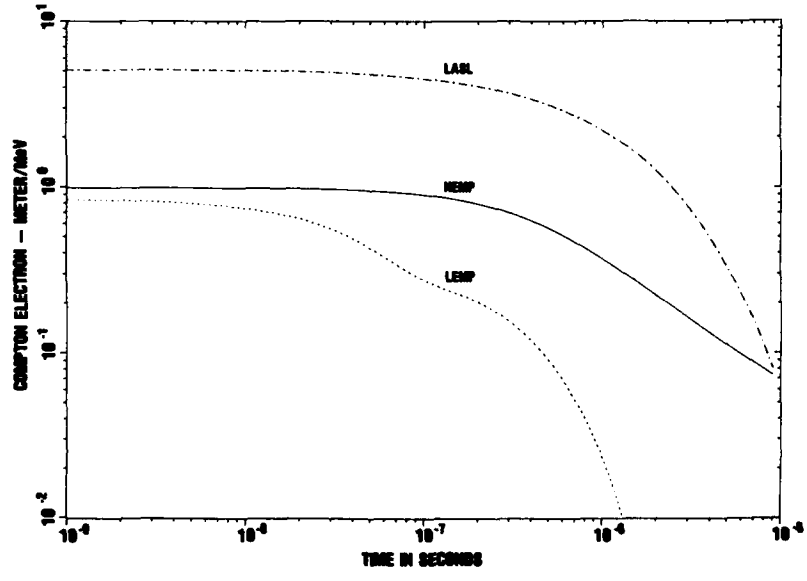

Figure 16. Time dependence compared for ratio of radial Compton electron current to energy deposition rate, at 3000-m range for 0.5-MeV gamma rays.

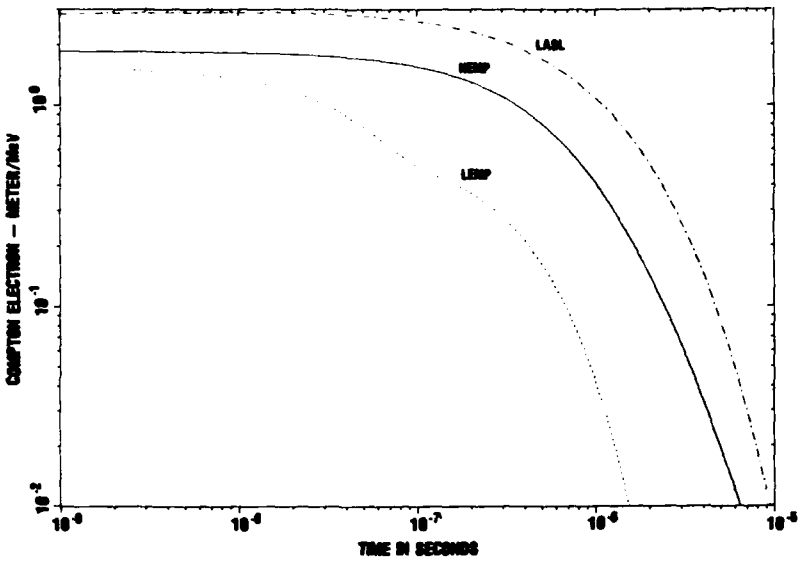

Figure 17. Time dependence compared for ratio of radial Compton electron current to energy deposition rate, at 3000-m range for 1.5-MeV gamma rays.

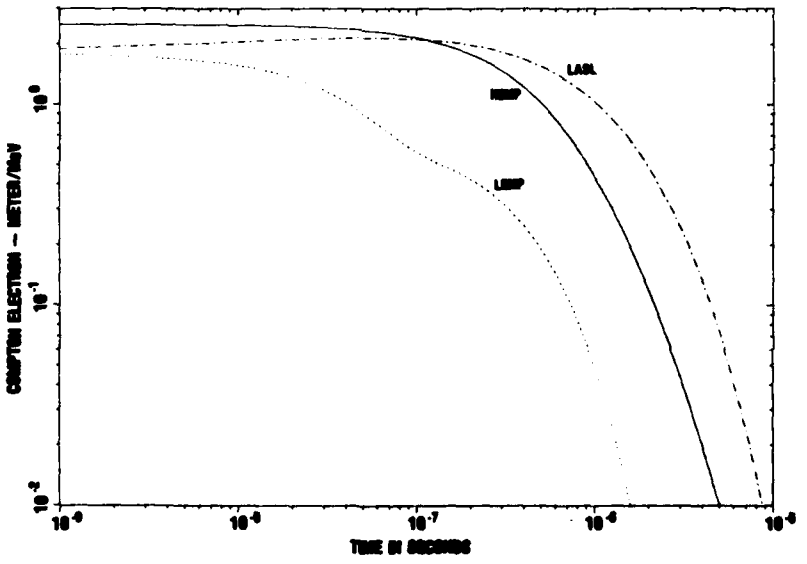

Figure 18. Time dependence compared for ratio of radial Compton electron current to energy deposition rate, at 3000-m range for 5.0-MeV gamma rays.

Agreement is worse at 3000 m for each gamma ray energy. The NEMP and LEMP curves are in fair agreement at early times, whereas the LASL curve is too high except for the 5.0-MeV curve. The LEMP curve decays much too fast, as expected at deep penetration where multiply scattered gamma rays retain more of their collimation than at shallow penetration. (The LEMP driver is based on shallow penetration data). The LASL curve, on the other hand, decays too slowly. Comparison of the NEMP curves with the Monte Carlo data that they were intended to fit reveals that the curves are usually somewhat too high after about 1 μs, up to a factor of about two. However, considering the steepness of the curve, this error is not serious. No doubt a more complicated functional form would approximate the Monte Carlo data more faithfully.

From these comparisons, LEMP drivers would underestimate the Compton current at 3000 m by about a factor of four at 100 ns after the gamma-dot peak, for any of the gamma ray energies considered. The LASL drivers should not be applied to gamma ray energies less than 1.0 MeV, and they also significantly overestimate the Compton current at 3000 m for 1.5 MeV.

No ground effect on the ratio of Compton current to energy deposition rate was identified.

7. CONCLUDING REMARKS

This report presents improved calculations of EMP drivers due to a gamma ray point source in air over ground and analytic approximations to these EMP drivers. These were done for seven source gamma ray energies from 0.5 to 7.0 MeV. The EMP driver calculations were based on Monte Carlo simulation of the gamma ray transport using the SLEDGE computer code developed for this study. Notable features of the simulation included tracking to 25 attenuation lengths (mean free paths) penetration, presence of the earth, use of correlated sampling to estimate Compton electron currents more accurately, and extensive use of biasing and importance functions. The theoretical basis of the SLEDGE code is discussed. Significant aspects of the Monte Carlo results also are discussed.

The analytic approximations to the EMP drivers are described in detail, including (1) the energy deposition buildup factor (both free field and ground influenced), (2) time dependence of energy deposition as a function of both range from the burst and nearness to the ground, (3) ratio of radial Compton electron current to energy deposition rate, and (4) theta Compton electron current due to the presence of the ground. These approximations have been incorporated into an EMP driver software package used with the NEMP near-surface-burst EMP environment prediction code. Comparisons are made with two previous EMP driver

packages, one used in the LEMP surface-burst EMP environment prediction code and the other originated by LASL scientists for high-altitude burst problems. Free-field agreement with the LEMP drivers was generally good at short ranges. Free-field agreement with the LASL drivers was better at higher gamma ray energies. The new results predict ground effects as well, which were not considered by the LEMP and LASL researchers.

◆◆

LITERATURE CITED

(1) H. J. Longley, C. L. Longmire, and K. S. Smith, Development of NEMP (U), Mission Research Corp., Santa Barbara, CA, HDL-CR-75-001-1 (April 1975). (SECRET--RESTRICTED DATA)

(2) H. J. Longley and K. S. Smith, Developments in NEMP for 1977 (U), Mission Research Corp., Santa Barbara, CA, HDL-CR-77-0022-1 (January 1978). (SECRET--RESTRICTED DATA)

(3) H. J. Longley and C. L. Longmire, Development and Testing of LEMP 1, Los Alamos Scientific Laboratory, NM, LA-4346 (April 1970).

(4) L. L. Carter and E. D. Cashwell, Particle-Transport Simulation with the Monte Carlo Method, U.S. Energy Research and Development Administration TID-26607 (1975).

(5) Milton Abramowitz and Irene Stegun, Handbook of Mathematical Functions, Dover Publications, Inc., New York (1965), 260.

(6) William T. Wyatt, Jr., Transmission Factor Effects on the Average Forward Range of Compton Electrons, Harry Diamond Laboratories HDL-TM-80-10 (January 1980).

(7) J. S. Malik, E. D. Cashwell, and R. G. Schrandt, The Time Dependence of the Compton Current and Energy Deposition from Scattered Gamma Rays, Los Alamos Scientific Laboratory, NM, LA-7386-MS (July 1978).

DISTRIBUTION

ADMINISTRATOR
DEFENSE DOCUMENTATION CENTER
ATTN DDC-TCA (12 COPIES)
CAMERON STATION, BUILDING 5
ALEXANDRIA, VA 22314

COMMANDER
US ARMY RSCH & STD GP (EUR)
ATTN LTC JAMES M. KENNEDY, JR.
CHIEF, PHYSICS & MATH BRANCH
FPO NEW YORK 09510

COMMANDER
US ARMY ARMAMENT MATERIEL
READINESS COMMAND
ATTN DRSAR-LEP-L, TECHNICAL LIBRARY
ROCK ISLAND, IL 61299

COMMANDER
US ARMY MISSILE & MUNITIONS
CENTER & SCHOOL
ATTN ATSK-CTD-F
REDSTONE ARSENAL, AL 35809

DIRECTOR
US ARMY MATERIEL SYSTEMS
ANALYSIS ACTIVITY
ATTN DRXSY-MP
ATTN DRXSY-PO
ABERDEEN PROVING GROUND, MD 21005

DIRECTOR
US ARMY BALLISTIC RESEARCH LABORATORY
ATTN DRDAR-TSB-S (STINFO)
ATTN DRXBR-AM, W. VANANTWERP
ATTN DRSTE-EL
ATTN DRDAR-BLE
ABERDEEN PROVING GROUND, MD 21005

U.S. ARMY ELECTRONICS TECHNOLOGY
AND DEVICES LABORATORY
ATTN DELET-DD
FORT MONMOUTH, NJ 07703

TEXAS INSTRUMENTS, INC.
P.O. BOX 226015
ATTN FRANK POBLENZ,
DALLAS, TX 75266

TELEDYNE BROWN ENGINEERING
CUMMINGS RESEARCH PARK
ATTN DR. MELVIN L. PRINCE, MS-44
HUNTSVILLE, AL 35807

ENGINEERING SOCIETIES LIBRARY
345 EAST 47TH STREET
ATTN ACQUISITIONS DEPARTMENT
NEW YORK, NY 10017

DIRECTOR
ARMED FORCES RADIOBIOLOGY RESEARCH
INSTITUTE
DEFENSE NUCLEAR AGENCY
NATIONAL NAVAL MEDICAL CENTER
ATTN RESEARCH PROGRAM COORDINATING
OFFICER
BETHESDA, MD 20014

ASSISTANT TO THE SECRETARY OF DEFENSE
ATOMIC ENERGY
ATTN EXECUTIVE ASSISTANT
WASHINGTON, DC 20301

DIRECTOR
DEFENSE ADVANCED RSCH PROJ AGENCY
ARCHITECT BUILDING
ATTN TIO
1400 WILSON BLVD.
ARLINGTON, VA 22209

DIRECTOR
DEFENSE CIVIL PREPAREDNESS AGENCY
ASSISTANT DIRECTOR FOR RESEARCH
ATTN ADMIN OFFICER
ATTN RE (EO)
ATTN PO (SE)
WASHINGTON, DC 20301

DEFENSE COMMUNICATIONS ENGINEERING
CENTER
ATTN CODE R720, C. STANSBERRY
ATTN CODE R123, TECH LIB
ATTN CODE R400
1860 WIEHLE AVENUE
RESTON, VA 22090

DIRECTOR
DEFENSE COMMUNICATIONS AGENCY
ATTN CCTC C312
ATTN CODE C313
WASHINGTON, DC 20305

DIRECTOR
DEFENSE INTELLIGENCE AGENCY
ATTN RDS-3A
ATTN RDS-3A4, POMPONIO PLAZA
WASHINGTON, DC 20301

DIRECTOR
DEFENSE NUCLEAR AGENCY
ATTN RATN
ATTN DDST
ATTN RAEV
ATTN TITL
ATTN STVL
ATTN VLIS
WASHINGTON, DC 20305

COMMANDER
FIELD COMMAND
DEFENSE NUCLEAR AGENCY
ATTN FCPR
ATTN FCSPM, J. SMITH
ATTN FCLMC
KIRTLAND AFB, NM 87115

DIRECTOR
INTERSERVICE NUCLEAR WEAPONS SCHOOL
ATTN TTV
KIRTLAND AFB, NM 87115

JOINT CHIEFS OF STAFF
ATTN J-3
WASHINGTON, DC 20301

DIRECTOR
JOINT STRATEGIC TARGET PLANNING
STAFF, JCS
OFFUTT AFB
ATTN JSAS
ATTN JPST
ATTN NRI-STINFO LIBRARY
OMAHA, NB 68113

CHIEF
LIVERMORE DIVISION
FIELD COMMAND DNA
DEPARTMENT OF DEFENSE
LAWRENCE LIVERMORE LABORATORY
P.O. BOX 808
ATTN FCPRL
LIVERMORE, CA 94550

NATIONAL COMMUNICATIONS SYSTEM
OFFICE OF THE MANAGER
DEPARTMENT OF DEFENSE
ATTN NCS-TS, CHARLES D. BODSON
WASHINGTON, DC 20305

DIRECTOR
NATIONAL SECURITY AGENCY
DEPARTMENT OF DEFENSE
ATTN R-52, O. VAN GUNTEN
ATTN S232, D. VINCENT
FT. MEADE, MD 20755

UNDER SECY OF DEF FOR RSCH & ENGRG
DEPARTMENT OF DEFENSE
ATTN G. BARSE
ATTN S&SS (OS)
WASHINGTON DC 20301

COMMANDER
BMD SYSTEM COMMAND
DEPARTMENT OF THE ARMY
P.O. BOX 1500
ATTN BMDSC-AOLIB
HUNTSVILLE, AL 35807

COMMANDER
ERADCOM TECHNICAL SUPPORT ACTIVITY
DEPARTMENT OF THE ARMY
ATTN DELCS-K, A COHEN
ATTN DELET-IR, E. HUNTER
FORT MONMOUTH, NJ 07703

COMMANDER
US ARMY ARMOR CENTER
ATTN TECHNICAL LIBRARY
FORT KNOX, KY 40121

COMMANDER
US ARMY COMM-ELEC ENGRG INSTAL
AGENCY
ATTN CCC-PRSO-S
ATTN CCC-CED-SES
FT HUACHUCA, AZ 85613

COMMANDER
US ARMY COMMUNICATIONS COMMAND
COMBAT DEVELOPMENT DIVISION
ATTN ATSI-CD-MD
FT. HUACHUCA, AZ 85613

CHIEF
US ARMY COMMUNICATIONS SYS AGENCY
ATTN CCM-RD-T CCM-AD-SV
FORT MONMOUTH, NJ 07703

PROJECT OFFICER
US ARMY COMMUNICATIONS RES &
DEV COMMAND
ATTN DRCPM-ATC
ATTN DRCPM-TDS-BSI
FORT MONMOUTH, NJ 07703

DIVISION ENGINEER
US ARMY ENGINEER DIV HUNTSVILLE
P.O. BOX 1600, WEST STATION
ATTN HNDED-SR
ATTN A. T. BOLT
HUNTSVILLE, AL 35807

US ARMY INTEL THREAT ANALYSIS
DETACHMENT
ROOM 2201, BLDG A
ARLINGTON HALL STATION
ATTN RM 2200, BLDG A
ARLINGTON, VA 22212

COMMANDER
US ARMY INTELLIGENCE & SEC CMD
ARLINGTON HALL STATION
4000 ARLINGTON BLVD
ATTN TECHNICAL LIBRARY
ATTN TECH INFO FAC
ARLINGTON, VA 22212

COMMANDER
US ARMY MISSILE RESEARCH
& DEVELOPMENT COMMAND
ATTN DRCPM-PE-EA, WALLACE O. WAGNER
ATTN DRCPM-PE-EG, WILLIAM B. JOHNSON
ATTN DRDMI-TBD
ATTN DRDMI-EAA
REDSTONE ARSENAL, AL 35809

US ARMY NUCLEAR & CHEMICAL AGENCY
7500 BACKLICK ROAD
BUILDING 2073
ATTN COL A. LOWRY
ATTN DR. J. BERBERET
SPRINGFIELD, VA 22150

COMMANDER
US ARMY TEST AND EVALUATION COMMAND
ATTN DRSTE-FA
ABERDEEN PROVING GROUND, MD 21005

COMMANDER
US ARMY TRAINING AND
DOCTRINE COMMAND
ATTN ATORI-OP-SW
FORT MONROE, VA 23651

COMMANDER
WHITE SANDS MISSILE RANGE
DEPARTMENT OF THE ARMY
ATTN STEWS-TE-AN, J. OKUMA
WHITE SANDS MISSILE RANGE, NM 88002

OFFICER-IN-CHARGE
CIVIL ENGINEERING LABORATORY
NAVAL CONSTRUCTION BATTALION CENTER
ATTN CODE L08A (LIBRARY)
ATTN CODE L08A
PORT HUENEME, CA 93041

COMMANDER
NAVAL AIR SYSTEMS COMMAND
ATTN AIR-350F
WASHINGTON, DC 21360

COMMANDER
NAVAL ELECTRONIC SYSTEMS COMMAND
ATTN PME 117-215
WASHINGTON, DC 20360

COMMANDER
NAVAL OCEAN SYSTEMS CENTER
ATTN CODE 015, C. FLETCHER
ATTN RESEARCH LIBRARY
ATTN CODE 7240, S. W. LICHTMAN
SAN DIEGO, CA 92152

COMMANDING OFFICER
NAVAL ORDNANCE STATION
ATTN STANDARDIZATION DIV
INDIAN HEAD, MD 20640

SUPERINTENDENT (CODE 1424)
NAVAL POSTGRADUATE SCHOOL
ATTN CODE 1424
MONTEREY, CA 93940

DIRECTOR
NAVAL RESEARCH LABORATORY
ATTN CODE 4104, EMANUAL L. BRANCATO
ATTN CODE 2627, DORIS R. FOLEN
ATTN CODE 6623, RICHARD L. STATLER
ATTN CODE 6624
WASHINGTON, DC 20375

COMMANDER
NAVAL SHIP ENGINEERING CENTER
DEPARTMENT OF THE NAVY
ATTN CODE 6174D2, EDWARD F. DUFFY
WASHINGTON, DC 20362

COMMANDER
NAVAL SURFACE WEAPONS CENTER
ATTN CODE F32, EDWIN R. RATHBURN
ATTN L. LIBELLO, CODE WR43
ATTN CODE WA51RH, RM 130-108
WHITE OAK, SILVER SPRING, MD 20910

COMMANDER
NAVAL SURFACE WEAPONS CENTER
DAHLGREN LABORAROTY
ATTN CODE DF-56
DAHLGREN, VA 22448

COMMANDER
NAVAL WEAPONS CENTER
ATTN CODE 533, TECH LIB
CHINA LAKE, CA 93555

COMMANDING OFFICER
NAVAL WEAPONS EVALUATION FACILITY
KIRTLAND AIR FORCE BASE
ATTN CODE AT-6
ALBUQUERQUE, NM 87117

OFFICE OF NAVAL RESEARCH
ATTN CODE 427
ARLINGTON, VA 22217

DIRECTOR
STRATEGIC SYSTEMS PROJECT OFFICE
NAVY DEPARTMENT
ATTN NSP-2701, JOHN W. PITSENBERGER
ATTN NSP-2342, RICHARD L. COLEMAN
ATTN NSP-43, TECH LIB
ATTN NSP-27334
ATTN NSP-230, D. GOLD
WASHINGTON, DC 20376

COMMANDER
AERONAUTICAL SYSTEMS DIVISION, AFSC
ATTN ASD-YH-EX
ATTN ENFTV
WRIGHT-PATTERSON AFB, OH 45333

AIR FORCE TECHNICAL APPLICATIONS
CENTER
ATTN TFS, M. SCHNEIDER
PATRICK AFB, FL 32925

AF WEAPONS LABORATORY, AFSC
ATTN NTN
ATTN NT
ATTN EL, CARL E. BAUM,
ATTN ELXT
ATTN SUL
ATTN CA
ATTN ELA, J. P. CASTILLO
ATTN ELP
ATTN ELT, W. PAGE
ATTN NXS
KIRTLAND AFB, NM 87117

DIRECTOR
AIR UNIVERSITY LIBRARY
DEPARTMENT OF THE AIR FORCE
ATTN AUL-LSE-70-250
MAXWELL AFB, AL 36112

HEADQUARTERS
ELECTRONIC SYSTEMS DEVISION/YSEA
DEPARTMENT OF THE AIR FORCE
ATTN YSEA
HANSCOM AFB, MA 01731

COMMANDER
FOREIGN TECHNOLOGY DIVISION, AFSC
ATTN NICD LIBRARY
ATTN ETDP, B. L. BALLARD
WRIGHT-PATTERSON AFB, OH 45433

COMMANDER
OGDEN ALC/MMEDDE
DEPARTMENT OF THE AIR FORCE
ATTN OO-ALC/MMETH, P. W. BERTHEL
ATTN MMEDO, LEO KIDMAN
ATTN MAJ R. BLACKBURN
HILL AFB, UT 84406

DISTRIBUTION (Cont'd)

COMMANDER
ROME AIR DEVELOPMENT CENTER AFSC
ATTN TSLD
GRIFFISS AFB, NY 13441

COMMANDER
SACRAMENTO AIR LOGISTICS CENTER
DEPARTMENT OF THE AIR FORCE
ATTN MMCRS, H. A. PELMASTRO
ATTN MMIRA, J. W. DEMES
ATTN MMSREM, F. R. SPEAR
MCCLELLAN AFB, CA 95652

SAMSO/IN
AIR FORCE SYSTEMS COMMAND
POST OFFICE BOX 92960
WORLDWAY POSTAL CENTER
(INTELLIGENCE)
ATTN IND
LOS ANGELES, CA 90009

SAMSO/MN
AIR FORCE SYSTEMS COMMAND
(MINUTEMAN)
ATTN MNNH, MAJ M. BARAN
ATTN MNNH, CAPT R. I. LAWRENCE
NORTON AFB, CA 92409

SAMSO/YA
AIR FORCE SYSTEMS COMMAND
POST OFFICE BOX 92960
WORLDWAY POSTAL CENTER
ATTN YAPC
LOS ANGELES, CA 90009

STRATEGIC AIR COMMAND/XPFS
ATTN NRI-STINFO LIBRARY
ATTN DEL
ATTN GARNET E. MATZKE
ATTN XPFS, MAJ BRIAN G. STEPHEN
OFFUTT AFB, NB 68113

DEPARTMENT OF ENERGY
ALBUQUERQUE OPERATIONS OFFICE
P.O. BOX 5400
ATTN DOC CON FOR TECH LIBRARY
ATTN OPERATIONAL SAFETY DIV
ALBUQUERQUE, NM 87115

UNIVERSITY OF CALIFORNIA
LAWRENCE LIVERMORE LABORATORY
P.O. BOX 808
ATTN DOC CON FOR TECHNICAL
INFORMATION DEPT
ATTN DOC CON FOR L-06, T. DONICH
ATTN DOC CON FOR L-545, D. MEEKER
ATTN DOC CON FOR L-156, E. MILLER
ATTN DOC CON FOR L-10, H. KRUGER
ATTN DOC CON FOR H. S. CABAYAN
LIVERMORE, CA 94550

LOS ALAMOS SCIENTIFIC LABORATORY
P.O. BOX 1663
ATTN DOC CON FOR BRUCE W. NOEL
ATTN DOC CON FOR CLARENCE BENTON
LOS ALAMOS, NM 87545

SANDIA LABORATORIES
P.O. BOX 5800
ATTN DON CON FOR C. N. VITTITOE
ATTN DON CON FOR R. L. PARKER
ATTN DOC CON FOR ELMER F. HARTMAN
ALBUQUERQUE, NM 87115

CENTRAL INTELLIGENCE AGENCY
ATTN RD/SI, RM 5G48, HQ BLDG
FOR OSI/NED/NWB
WASHINGTON, DC 20505

ADMINISTRATOR
DEFENSE ELECTRIC POWER ADMIN
DEPARTMENT OF THE INTERIOR
INTERIOR SOUTH BLDG, 312
ATTN L. O'NEILL
WASHINGTON, DC 20240

DEPARTMENT OF TRANSPORTATION
FEDERAL AVIATION ADMINISTRATION
HEADQUARTERS SEC DIV, ASE-300
800 INDEPENDENCE AVENUE, SW
ATTN SEC DIV ASE-300
WASHINGTON, DC 20591

AEROSPACE CORPORATION
P.O. BOX 92957
ATTN C. B. PEARLSTON
ATTN IRVING M. GARFUNKEL
ATTN JULIAN REINHEIMER
ATTN LIBRARY
ATTN CHARLES GREENHOW
LOS ANGELES, CA 90009

AGBABIAN ASSOCIATES
250 NORTH NASH STREET
ATTN LIBRARY
EL SEGUNDO, CA 90245

AVCO RESEARCH & SYSTEMS GROUP
201 LOWELL STREET
ATTN W. LEPSEVICH
WILMINGTON, MA 01887

BATTELLE MEMORIAL INSTITUTE
505 KING AVENUE
ATTN ROBERT H. BALZEK
ATTN EUGENE R. LEACH
COLUMBUS, OH 43201

BDM CORPORATION
7915 JONES BRANCH DRIVE
ATTN CORPORATE LIBRARY
MCLEAN, VA 22101

BDM CORPORATION
P.O. BOX 9274
ALBUQUERQUE INTERNATIONAL
ATTN LIB
ALBUQUERQUE, NM 87119

BENDIX CORPORATION, THE
RESEARCH LABORATORIES DIVISION
BENDIX CENTER
ATTN MAX FRANK
SOUTHFIELD, MI 48075

BENDIX CORPORATION
NAVIGATION AND CONTROL GROUP
ATTN DEPT 6401
TETERBORO, NJ 07608

BOEING COMPANY
P.O. BOX 3707
ATTN HOWARD W. WICKLEIN
ATTN D. E. ISBELL
ATTN DAVID KEMLE
ATTN B. C. HANRAHAN
ATTN KENT TECH LIB
SEATTLE, WA 98124

BOOZ-ALLEN AND HAMILTON, INC.
106 APPLE STREET
ATTN R. J. CHRISNER
ATTN TECH LIB
TINTON FALLS, NJ 07724

BURROUGHS CORPORATION
FEDERAL AND SPECIAL SYSTEMS GROUP
CENTRAL AVE AND ROUTE 252
P.O. BOX 517
ATTN ANGELO J. MAURIELLO
PAOLI, PA 19301

CALSPAN CORPORATION
P.O. BOX 400
ATTN TECH LIBRARY
BUFFALO, NY 14225

CHARLES STARK DRAPER LABORATORY INC.
555 TECHNOLOGY SQUARE
ATTN KENNETH FERTIG
ATTN TIC MS 74
CHAMBRIDGE, MA 02139

CINCINNATI ELECTRONICS CORPORATION
2630 GLENDALE-MILFORD ROAD
ATTN LOIS HAMMOND
CINCINNATI, OH 45241

COMPUTER SCIENCES CORPORATION
6565 ARLINGTON BLVD
ATTN RAMONA BRIGGS
FALLS CHURCH, VA 22046

COMPUTER SCIENCES CORPORATION
1400 SAN MATEO BLVD, SE
ATTN RICHARD H. DICKHAUT
ATTN ALVIN SCHIFF
ALBUQUERQUE, NM 87108

CONTROL DATA CORPORATION
P.O. BOX O
ATTN JACK MEEHAN
MINNEAPOLIS, MN 55440

CUTLER-HAMMER, INC.
AIL DIVISION
COMAC ROAD
ATTN EDWARD KARPEN
DEER PARK, NY 11729

DIKEWOOD INDUSTRIES, INC
1009 BRANDBURY DRIVE, SE
ATTN TECH LIB
ATTN L. WAYNE DAVIS
ALBUQUERQUE, NM 87106

DIKEWOOD INDUSTRIES, INC.
1100 GLENDON AVENUE
ATTN K. LEE
LOS ANGELES, CA 90024

E-SYSTEMS, INC
GREENVILLE DIVISION
P.O. BOX 1056
ATTN JOLETA MOORE
GREENVILLE, TX 75401

EFFECTS TECHNOLOGY, INC.
5383 HOLLISTER AVENUE
ATTN S. CLOW
SANTA BARBARA, CA 93111

EG&G WASHINGTON ANALYTICAL
SERVICES CENTER, INC.
P.O. BOX 10218
ATTN C. GILES
ALBUQUERQUE, NM 87114

EXXON NUCLEAR COMPANY, INC.
RESEARCH AND TECHNOLOGY CENTER
2955 GEORGE WASHINGTON WAY
ATTN DR, A. W. TRIVELPIECE
RICHLAND, WA 99352

FAIRCHILD CAMERA AND INSTRUMENT CORP
464 ELLIS STREET
ATTN SEC CON FOR DAVID K. MYERS
MOUNTAIN VIEW, CA 94040

FORD AEROSPACE & COMMUNICATIONS CORP
3939 FABIAN WAY
ATTN TECHNICAL LIBRARY
PALO ALTO, CA 94303

FORD AEROSPACE & COMMUNICATIONS OPERATIONS
FORD & JAMBOREE ROADS
ATTN KEN C. ATTINGER
ATTN E. R. PONCELET, JR.
NEWPORT BEACH, CA 92663

FRANKLIN INSTITUTE, THE
20TH STREET AND PARKWAY
ATTN RAMIE H. THOMPSON
PHILADELPHIA, PA 19103

GENERAL DYNAMICS CORP
ELECTRONICS DIVISION
P.O. BOX 81125
ATTN RSCH LIB
SAN DIEGO, CA 92138

GENERAL DYNAMICS CORPORATION
INTER-DIVISION RESEARCH LIBRARY
KEARNY MESA
P.O. BOX 80847
ATTN RESEARCH LIBRARY
SAN DIEGO, CA 98123

GENERAL ELECTRIC CO.-TEMPO
CENTER FOR ADVANCED STUDIES
816 STATE STREET (PO DRAWER QQ)
ATTN DASIAC
ATTN ROYDEN R. RUTHERFORD
ATTN WILLIAM MCNAMERA
SANTA BARBARA, CA 93102

GENERAL ELECTRIC COMPANY
AEROSPACE ELECTRONICS SYSTEMS
FRENCH ROAD
ATTN CHARLES M. HEWISON
UTICA, NY 13503

GENERAL ELECTRIC COMPANY
P.O. BOX 5000
ATTN TECH LIB
BINGHAMTON, NY 13902

GENERAL ELECTRIC CO.-TEMPO
ALEXANDRIA OFFICE
HUNTINGTON BUILDING, SUITE 300
2560 HUNTINGTON AVENUE
ATTN DASIAC
ALEXANDRIA, VA 22303

GENERAL RESEARCH CORPORATION
SANTA BARBARA
P.O. BOX 6770
ATTN TECH INFO OFFICE
SANTA BARBARA, CA 93111

GEORGIA INSTITUTE OF TECHNOLOGY
GEORGIA TECH RESEARCH INSTITUTE
ATTN R. CURRY
ATLANTA, GA 30332

GEORGIA INSTITUTE OF TECHNOLOGY
OFFICE OF CONTRACT ADMINISTRATION
ATTN RES & SEC COORD FOR HUGH DENNY
ATLANTA, GA 30332

GRUMMAN AEROSPACE CORPORATION
SOUTH OYSTER BAY ROAD
ATTN L-01 35
BETHPAGE, NY 11714

GTE SYLVANIA INC.
ELECTRONICS SYSTEMS GRP-EASTERN DIV
77 A STREET
ATTN CHARLES A. THORNHILL, LIBRARIAN
ATTN LEONDARD L. BLAISDELL
NEEDHAM, MA 02194

GTE SYLVANIA, INC.
189 B STREET
ATTN CHARLES H. RAMSBOTTOM
ATTN DAVID D. FLOOD
ATTN EMIL P. MOTCHOK
ATTN H & V GROUP, MARIO A. NUREFORA
ATTN J. WALDRON
NEEDHAM HEIGHTS, MA 02194

HARRIS CORPORATION
HARRIS SEMICONDUCTOR DIVISION
P.O. BOX 883
ATTN V PRES & MGR PRGMS DIV
MELBOURNE, FL 32901

HAZELTINE CORPORATION
PULASKI ROAD
ATTN TECH INFO CTR, M. WAITE
GREENLAWN, NY 11740

HONEYWELL INCORPORATED
AVIONICS DIVISION
2600 RIDGEWAY PARKWAY
ATTN S&RC LIB
ATTN RONALD R. JOHNSON
MINNEAPOLIS, MN 55413

HONEYWELL INCORPORATED
AVIONICS DIVISION
13350 U.S. HIGHWAY 19 NORTH
ATTN M.S 725-5, STACEY H. GRAFF
ATTN W. E STEWART
ST. PETERSBURG, FL 33733

HUGHES AIRCRAFT COMPANY
CENTINELA AND TEALE
ATTN JOHN B. SINGLETARY
ATTN CTDC 6/E110
ATTN KENNETH R. WALKER
CULVER CITY, CA 90230

IIT RESEARCH INSTITUTE
ELECTROMAG COMPATABILITY ANAL CTR
NORTH SEVERN
ATTN ACOAT
ANNAPOLIS, MD 21402

IIT RESEARCH INSTITUTE
10 WEST 35TH STREET
ATTN IRVING N. MINDEL
ATTN JACK E. BRIDGES
CHICAGO, IL 60616

INSTITUTE FOR DEFENSE ANALYSES
400 ARMY-NAVY DRIVE
ATTN TECH INFO SERVICES
ARLINGTON, VA 22202

INTL TEL & TELEGRAPH CORPORATION
500 WASHINGTON AVENUE
ATTN TECHNICAL LIBRARY
ATTN ALEXANDER T. RICHARDSON
NUTLEY, NJ 07110

IRT CORPORATION
P.O. BOX 81087
ATTN C. B. WILLIAMS
ATTN DENNIS SWIFT
SAN DIEGO, CA 92138

JAYCOR
SANTA BARBARA FACILITY
P.O. BOX 2008
ATTN W. A. RADASKY
SANTA BARBARA, CA 93120

JAYCOR
1401 CAMINO DEL MAR
ATTN ERIC P. WENAAS
ATTN RALPH H. STAHL
DEL MAR, CA 92014

JAYCOR
205 S WHITING STREET, SUITE 500
ATTN LIB
ALEXANDRIA, VA 22304

KAMAN SCIENCES CORPORATION
1500 GARDEN OF THE GODS ROAD
ATTN ALBERT P. BRIDGES
ATTN W. FOSTER RICH
ATTN WALTER E. WARE
ATTN FRANK H. SHELTON
ATTN JERRY I. LUBELL
ATTN PHIL TRACY
ATTN WERNER STARK
COLORADO SPRINGS, CO 80907

LITTON SYSTEMS, INC.
DATA SYSTEMS DIVISION
8000 WOODLEY AVENUE
ATTN EMC GP
ATTN M848-61
VAN NUYS, CA 91409

LITTON SYSTEMS, INC.
AMECOM DIVISION
5115 CALVERT ROAD
ATTN J. SKAGGS
COLLEGE PARK, MD 20740

LOCKHEED MISSLES AMD SPACE COMPANY, INC
P.O. BOX 504
ATTN L. ROSSI
ATTN SAMUEL I. TAIMUTY
ATTN H. E. THAYN
ATTN GEORGE F. HEATH
ATTN BENJAMIN T. KIMURA
SUNNYVALE, CA 94086

LOCKHEED MISSILES AND SPACE COMPANY, INC.
3251 HANOVER STREET
ATTN TECH INFO CTR D/COLL
PALO ALTO, CA 94304

M.I.T. LINCOLN LABORATORY
P.O. BOX 73
ATTN LEONA LOUGHLIN
LEXINGTON, MA 02173

MARTIN MARIETTA CORPORATION
ORLANDO DIVISION
P.O. BOX 5837
ATTN MONA C. GRIFFITH
ORLANDO, FL 32805

MCDONNEL DOUGLAS CORPORATION
POST OFFICE BOX 516
ATTN TOM ENDER
ST. LOUIS, MO 63166

MCDONNELL DOUGLAS CORPORATION
5301 BOLSA AVENUE
ATTN STANLEY SCHNEIDER
ATTN TECH LINRARY SERVICES
HUNTINGTON BEACH, CA 92647

MISSION RESEARCH CORPORATION
P.O. DRAWER 719
ATTN EMP GROUP
ATTN WILLIAM C. HART
ATTN C. LONGMIRE
SANTA BARBARA, CA 93102

MISSION RESEARCH CORPORATION
EM SYSTEM APPLICATIONS DIVISION
1400 SAN MATEO BLVD, SE, SUITE A
ATTN DAVID E. MEREWETHER
ATTN L. N. MCCORMICK
ALBUQUERQUE, NM 87108

MISSION RESEARCH CORPORATION-SAN DIEGO
P.O. BOX 1209
ATTN V. A. J. VAN LINT
LA JOLLA, CA 92038

MITRE CORPORATION, THE
P.O. BOX 208
ATTN M. F. FITZGERALD
BEDFORD, MA 01730

NORDEN SYSTEMS, INC.
HELEN STREET
ATTN TECHNICAL LIBRARY
NORWALK, CT 06856

NORTHROP RESEARCH TECHNOLOGY CENTER
ONE RESEARCH PARK
ATTN LIBRARY
PALOS VERDES PENN, CA 90274

NORTHROP CORPORTION
ELECTRONIC DIVISION
2301 WEST 120TH STREET
ATTN LEW SMITH
ATTN RAD EFFECTS GRP
HAWTHORNE, CA 90250

PHYSICS INTERNATIONAL COMPANY
2700 MERCED STREET
ATTN DOC CON
SAN LEANDRO, CA 94577

R.&.D ASSOCIATED
P.O. BOX 9695
ATTN S. CLAY ROGERS
ATTN RICHARD R. SCHAEFER
ATTN DOC CON
ATTN M. GROVER
ATTN C. MACDONALD
MARINA DEL REY, CA 90291

R&D ASSOCIATES
1401 WILSON BLVD
SUITE 500
ATTN J. BOMBARDT
ARLINGTON, VA 22209

RAND CORPORATION
1700 MAIN STREET
ATTN LIB-D
ATTN W. SOLLFREY
SANTA MONICA, CA 90406

RAYTHEON COMPANY
HARTWELL ROAD
ATTN GAJANAN H. JOSI
BEDFORD, MA 01730

RAYTHEON COMPANY
528 BOSTON POST ROAD
ATTN HAROLD L. FLESCHER
SUDBURY, MA 01776

RCA CORPORATION
GOVERNMENT SYSTEMS DIVISION
ASTRO ELECTRONICS
P.O. BOX 800, LOCUST CORNER
EAST WINDSOR TOWNSHIP
PRINCETON, NJ 08540

RCA CORPORATION
DAVID SARNOFF RESEARCH CENTER
P.O. BOX 432
ATTN SECURITY DEPT, L. MINICH
PRINCETON, NJ 08540

RCA CORPORATION
CAMDEN COMPLEX
FRONT & COOPER STREETS
ATTN OLIVE WHITEHEAD
ATTN R. W. TOSTROM
CAMDEN, NJ 08012

ROCKWELL INTERNATIONAL CORPORATION
P.O. BOX 3105
ATTN N. J. RUDIE
ATTN J. L. MONROE
ATTN V. J. MICHEL
ATTN D/243-068, 031-CA31
ANAHEIM, CA 92803

ROCKWELL INTERNATIONAL CORPORATION
SPACE DIVISION
12214 SOUTH LAKEWOOD BOULEVARD
ATTN B. E. WHITE
DOWNEY, CA 90241

ROCKWELL INTERNATIONAL CORPORATION
815 LAPAHM STREET
ATTN B-1, DIV TIC (BAOB)
EL SEGUNDO, CA 90245

ROCKWELL INTERNATIONAL CORPORATION
P.O. BOX 369
ATTN F. A. SHAW
CLEARFIELD, UT 84015

SANDERS ASSOCIATES, INC.
95 CANAL STREET
ATTN 1-6270, R. G. DESPATHY, SR P E
NASHUA, NH 03060

SCIENCE APPLICATIONS, INC.
P.O. BOX 277
ATTN FREDERICK M. TESCHE
BERKELEY, CA 94701

SCIENCE APPLICATIONS, INC.
P.O. BOX 2351
ATTN R. PARKINSON
LA JOLLA, CA 92038

SCIENCE APPLICATIONS, INC.
HUNTSVILLE DIVISION
2109 W. CLINTON AVENUE
SUITE 700
ATTN NOEL R. BYRN
HUNTSVILLE, AL 35805

SCIENCE APPLICATIONS, INC.
8400 WESTPARK DRIVE
ATTN WILLIAM L. CHADSEY
MCLEAN, VA 22101

SINGER COMPANY
ATTN: SECURITY MANAGER
FOR TECH INFO CTR
1150 MC BRIDE AVENUE
LITTLE FALLS, NJ 07424

SPERRY RAND CORPORATION
SPERRY MICROWAVE ELECTRONICS
P.O. BOX 4648
ATTN MARGARET CORT
CLEARWATER, FL 33518

SPERRY RAND CORPORATION
SPERRY DIVISION
MARCUS AVENUE
ATTN TECH LIB
GREAT NECK, NY 11020

SPERRY RAND CORPORATION
SPERRY FLIGHT SYSTEMS
P.O. BOX 21111
ATTN D. ANDREW SCHOW
PHOENIX, AZ 85036

SPIRE CORPORATION
P.O. BOX D
ATTN JOHN R. UGLUM
ATTN ROGER G. LITTLE
BEDFORD, MA 01730

SRI INTERNATIONAL
333 RAVENSWOOD AVENUE
ATTN ARTHUR LEE WHITSON
MENLO PARK, CA 94025

SYSTEMS, SCIENCE AND SOFTWARE, INC.
P.O. BOX 1620
ATTN ANDREW R. WILSON
LA JOLLA, CA 92038

TEXAS INSTRUMENTS, INC.
P.O. BOX 6015
ATTN TECH LIB
ATTN DONALD J. MANUS
DALLAS, TX 75265

TRW DEFENSE & SPACE SYS GROUP
ONE SPACE PARK
ATTN O. E. ADAMS
ATTN R. K. PLEBUCH
ATTN L. R. MAGNOLIA
ATTN H. H. HOLLOWAY
ATTN W. GARGARO
REDONDO BEACH, CA 90278

TEXAS TECH UNIVERSITY
P.O. BOX 5404 NORTH COLLEGE STATION
ATTN TRAVIS L. SIMPSON
LUBBOCK, TX 79417

UNITED TECHNOLOGIES CORP
HAMILTON STANDARD DIVISION
BRADLEY INTERNATIONAL AIRPORT
ATTN CHIEF ELEC DESIGN
WINDSOR LOCKS, CT 06069

WESTINGHOUSE ELECTRIC CORPORATION
ADVANCED ENERGY SYSTEMS DIV
P.O. BOX 10864
ATTN TECH LIB
PITTSBURGH, PA 15236

US ARMY ELECTRONICS RESEARCH
& DEVELOPMENT COMMAND
ATTN TECHNICAL DIRECTOR, DRDEL-CT

HARRY DIAMOND LABORATORIES
ATTN CO/TD/TSO/DIVISION DIRECTORS
ATTN RECORD COPY, 81200
ATTN HDL LIBRARY 81100 (3 COPIES)
ATTN HDL LIBRARY (WOODBRIDGE) 81100
ATTN TECHNICAL REPORTS BRANCH, 81300
ATTN CHAIRMAN, EDITORIAL COMMITTEE
ATTN CHIEF, 21000
ATTN CHIEF, 22000
ATTN CHIEF, 22100 (3 COPIES)
ATTN CHIEF, 22300
ATTN CHIEF, 22800
ATTN CHIEF, 22900
ATTN CHIEF, 13300
ATTN CHIEF, 21100 (3 COPIES)
ATTN CHIEF, 21200
ATTN CHIEF, 21300 (5 COPIES)
ATTN CHIEF, 21400 (2 COPIES)
ATTN CHIEF, 21500
ATTN BALICKI, F. W., 20240
ATTN WIMENITZ, F. N., 20240
ATTN TALLERICO, A., 47400
ATTN BIXBY, R., 22900
ATTN WYATT, W. T., 21300 (20 COPIES)